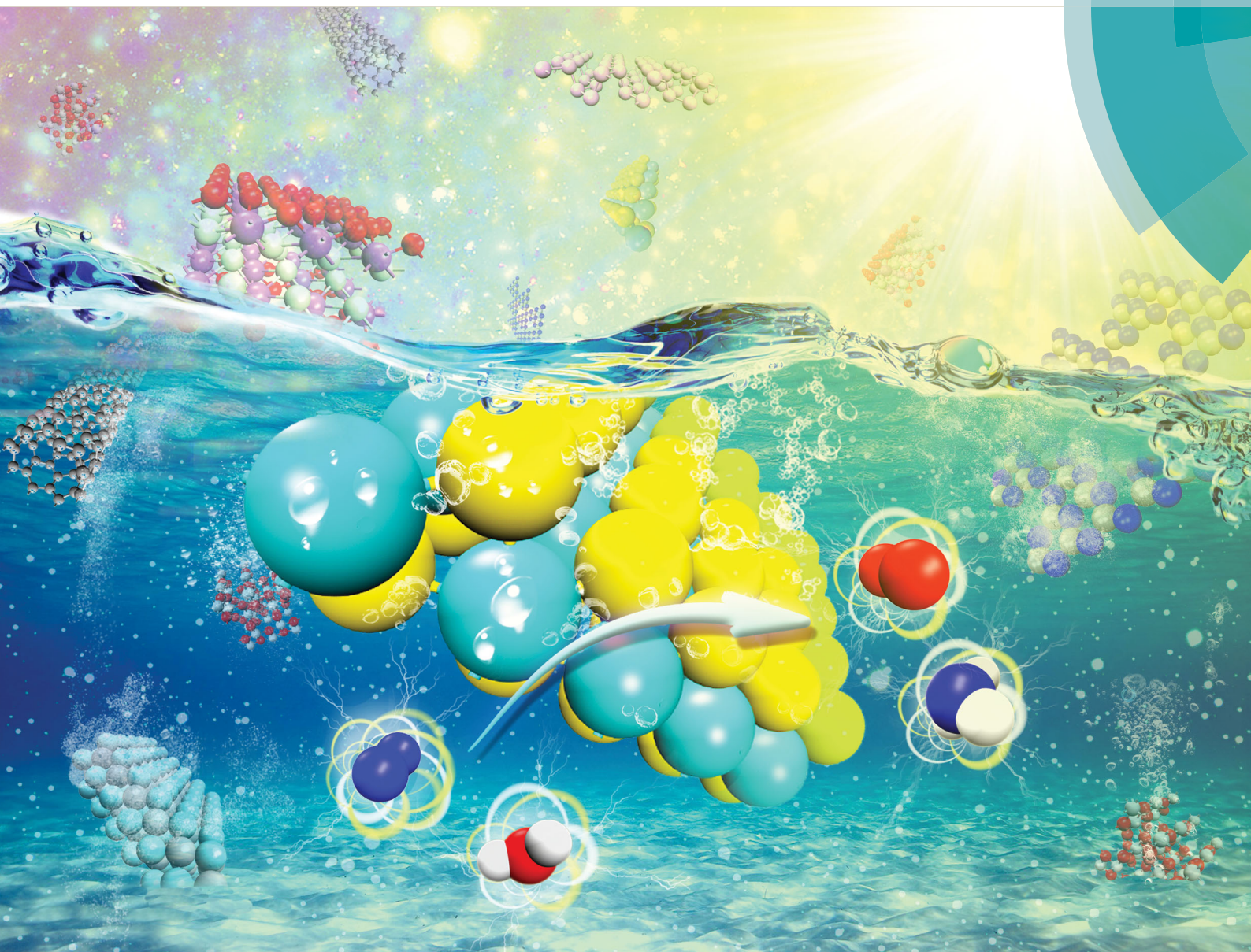


Materials Horizons

rsc.li/materials-horizons



ISSN 2051-6347



REVIEW ARTICLE



Neng Li, Wee-Jun Ong *et al.*

Photocatalytic fixation of nitrogen to ammonia: state-of-the-art advancements and future prospects



Cite this: *Mater. Horiz.*, 2018,
5, 9

Photocatalytic fixation of nitrogen to ammonia: state-of-the-art advancements and future prospects

Xingzhu Chen,^a Neng Li,^{*ab} Zhouzhou Kong,^a Wee-Jun Ong ^{*c} and
Xiujian Zhao ^a

The burgeoning development of ammonia (NH₃) synthesis technology addresses the urgency of food intake required to sustain the population growth of the last 100 years. To date, NH₃ has mostly been synthesized by the Haber–Bosch process in industry. Under the ever-increasing pressure of the fossil fuel depletion crisis and anthropogenic global climate change with continuous CO₂ emission in the 21st century, research targeting the synthesis of NH₃ under mild conditions in a sustainable and environment friendly manner is vigorous and thriving. Therefore, the focus of this review is the state-of-the-art engineering of efficient photocatalysts for dinitrogen (N₂) fixation toward NH₃ synthesis. Strenuous efforts have been devoted to modifying the intrinsic properties of semiconductors (*i.e.* poor electron transport, rapid electron–hole recombination and sluggish reaction kinetics), including nanoarchitecture design, crystal facet engineering, doping and heterostructuring. Herein, this review provides insights into the most recent advancements in understanding the charge carrier kinetics of photocatalysts with respect to charge transfer, migration and separation, which are of fundamental significance to photocatalytic N₂ fixation. Subsequently, the challenges, outlooks and future prospects at the forefront of this research platform are presented. As such, it is anticipated that this review will shed new light on photocatalytic N₂ fixation and NH₃ synthesis and will also provide a blueprint for further investigations and momentous breakthroughs in next-generation catalyst design.

Received 20th July 2017,
Accepted 29th August 2017

DOI: 10.1039/c7mh00557a

rsc.li/materials-horizons

1. Introduction

It is a well known fact that nitrogen is one of the starting building blocks for the synthesis of amino acids, nucleotides and other major biological compounds in all organisms.^{1,2} The main source of nitrogen, dinitrogen (N₂), is the largest single component of the Earth's atmosphere (around 78% by volume). As an important precursor for nitrogen-containing compounds, ammonia (NH₃) could be directly synthesized from dinitrogen by a small group of organisms named diazotrophs in nature.³ However, this could scarcely meet the large needs of the fertilizer industry today.

The fixation of N₂ to NH₃ is thermodynamically accessible: $\text{N}_{2(\text{g})} + 3\text{H}_{2(\text{g})} \rightarrow 2\text{NH}_{3(\text{g})}$, $\Delta H_{298\text{K}} = -92.2 \text{ kJ mol}^{-1}$. However, this

reaction cannot occur spontaneously under ambient conditions. The reduction reactions of N₂ to its partial reduzates, such as diazene (N₂H₂) or hydrazine (N₂H₄), are also non-spontaneous due to the positive standard enthalpies of formation of +212.9 and +95.35 kJ mol^{−1} for N₂H₂ and N₂H₄, respectively.⁴ There are many factors hindering the cleavage and hydrogenation of dinitrogen in nature. First, the thermodynamically strong cleavage energy of the first bond in N₂ (410 kJ mol^{−1}) manifests the critical challenge in the full dissociation of N≡N, which explains the chemical inactivity of N₂ compared to other triple-bonded molecules.⁵ Additionally, from the aspect of kinetics, the large energy gap between the HOMO (the σ_g2p bonding orbital) and LUMO (the π_g*2p anti-bonding orbital) explains the high chemical stability of N₂. Other factors, such as low proton affinity, also account for the difficulty of direct protonation of N₂. Detailed descriptions can be found in the review article by Jia and Quadrelli.⁴

The Haber–Bosch process, which involves the reaction of N₂ and hydrogen (H₂) over iron or ruthenium-based catalysts, has been estimated to be one of the most intriguing discoveries of the last century.^{6,7} After 100 years of development, the temperature is controlled to near 450 °C and the reaction pressure has decreased

^a State Key Laboratory of Silicate Materials for Architectures, Wuhan University of Technology, Hubei, 430070, China. E-mail: lineng@whut.edu.cn

^b Department of Materials Science & Metallurgy, University of Cambridge, Cambridge, CB3 0FS, UK

^c Institute of Materials Research and Engineering (IMRE), Agency for Science, Technology and Research (A*STAR), 2 Fusionopolis Way, Innovis, Singapore 138634, Singapore. E-mail: ongwj@imre.a-star.edu.sg, ongweejun@gmail.com; Web: <https://sites.google.com/site/wjongresearch/>

to 15 to 30 MPa from the original 50 to 100 MPa, while the efficiency is limited to 10% to 15%.^{8,9} Inevitably, this process accounts for 1.6% of total global CO₂ emissions; this is attributed to the presence of hydrocarbons in the raw materials (as the main hydrogen source and energy supplier in this process).¹⁰

Parallel to the optimization of the thermocatalytic process,^{11–14} several other methods have aroused widespread attention in the synthesis of ammonia to date. Before we engage in our topic of photocatalysis for the fixation of nitrogen to ammonia, we would like to briefly mention the progress of the other two traditional approaches. Owing to the variable coordination number of transition metals, organometallic complexes can participate in the activation of N₂. The ground-breaking work of the first nitrogen complex [Ru(NH₃)₅(N₂)]⁺ in 1965 challenged the traditional belief that dinitrogen cannot form complexes.¹⁵ Since then, nitrogen

complexes have been developed to generate ammonia under particular conditions, in which central elements of various transition metals, such as molybdenum,^{16–18} iron and titanium,^{19–22} were tested as the sites of dinitrogen coordination and reduction. Furthermore, the model and action mechanism of iron molybdenum complexes as active sites in nitrogenase enzymes have greatly fascinated many chemists and biologists.^{23–25} On the other hand, inspired by electron and proton transfer processes, numerous researchers have carried out investigations of electrochemical and electrocatalytic approaches.²⁶ Since a solid electrolyte cell was first used in the electrochemical synthesis of ammonia in 1998,²⁷ various conducting ceramic membranes have been tested to produce NH₃ from N₂.^{28–31} Since then, polymer electrolytes such as Nafion and sulfonated polysulfone have been deemed to provide excellent proton conductivity under low temperature.^{32–34} Later, molten salts such as chlorides,³⁵ oxide-carbonates or hydroxides were employed as electrolytes.^{36–39} Very recently, Chen *et al.* reported an electrolyte-less cell with the highest faradaic efficiency of 95.1% and a relatively low rate of $3.60 \times 10^{-12} \text{ mol s}^{-1} \text{ cm}^{-2}$ at room temperature, wherein the electrocatalyst was based on Fe₂O₃ nanoparticles supported on conductive carbon nanotubes (Fe₂O₃-CNT).⁴⁰

With regard to the inexhaustible and clean solar energy from sunlight,^{41–47} photocatalysis has been thrust into the limelight in the realms of energy and chemical fuel production; thus, blossoming interest in the design of myriad semiconductors has been witnessed in recent years.^{48–60} Generally, the photocatalytic process makes use of photons as the driving force to propel the activation of N₂. Compared with electrochemical



Xingzhu Chen

Xingzhu Chen received her BS in Materials Science and Engineering from Wuhan University of Technology in 2016. She is presently working on her PhD at Wuhan University of Technology. Her research interests include photo-electrochemistry, photocatalysis, and the development of photocatalysts, related materials and devices.



Neng Li

Neng Li received his PhD degree in condensed matter physics from Huazhong University of Science and Technology in 2011. He then joined the Shenzhen Institutes of Advanced Technology, Chinese Academy of Sciences as a Research Fellow in 2011. He worked at the Department of Physics and Astronomy, University of Missouri-Kansas City as a postdoctoral researcher from 2012 to 2014. In 2015, he joined Wuhan University of Technology as a Full

Professor. Dr Li was a Visiting Research Fellow at the Department of Materials Science & Metallurgy, University of Cambridge, UK from 2016 to 2017. His research interests focus on energy and environmental applications such as photocatalysis, photocatalytic hydrogen production, CO₂ reduction, N₂ fixation, and the development of hybrid functional materials and related devices.

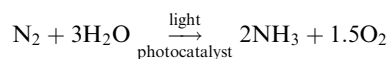


Wee-Jun Ong

*Wee-Jun Ong received his BE and PhD degrees in Chemical Engineering from Monash University. In 2015, he was a Visiting Research Fellow at the University of New South Wales and Monash University Clayton Campus, Australia. He is currently a Research Scientist at IMRE, A*STAR in Singapore. At present, he serves as the Associate Editor of Frontiers in Materials, an Editorial Board Member of Scientific Reports, Nanotechnology*

and Nano Futures, and a Community Board Member of Materials Horizons. He has also been the Lead Guest Editor of several Special Issues. His research interests primarily focus on photocatalytic, photoelectrochemical and electrochemical H₂O splitting, CO₂ reduction and N₂ fixation for energy conversion and storage using two-dimensional (2D)-based nanomaterials, transition metal dichalcogenides/phosphides and carbonaceous-based hybrid nanocomposites. For more details, see <https://sites.google.com/site/wjongresearch/>.

approaches, photon-driven fixation of N_2 has reached a stumbling block stemming from the difficulties of N_2 chemisorption and activation.⁶¹ The magnitudes of production rates for most studied photocatalysts remain below par,⁶² distinctly hindering the success of the solar fixation of N_2 . In the initial studies, N_2 photoreduction was considered to take place in nature over abundant minerals on the surface of the earth; thus, earlier studies on the photocatalytic fixation of N_2 mainly focused on soil minerals and sand in nature.^{63–65} This was introduced in the previous work of Schrauzer.⁶⁶ Since the first exploratory study on as-synthesized TiO_2 -based photocatalysts for N_2 fixation under UV light in 1977,⁶⁷ a flurry of research activities have been devoted to the development of photocatalytic N_2 fixation, especially in the 21st century, due to the fact that the driving force (light) and ingredients (water and air) of this process are relatively clean, cheap and accessible, as shown in the following equation.



The thermodynamic non-spontaneous reaction, which can be regarded as a combination of water splitting and N_2 fixation, can be accomplished with the introduction of solar energy.

To the best of our knowledge, there is no literature pertaining to the latest research progress of photocatalytic N_2 fixation with respect to the classification of photocatalysts. In this review article, we will present and update the state-of-the-art research advancements in this growing field of N_2 fixation, as depicted in Fig. 1. Briefly, the classification of pristine photocatalysts is firstly discussed, followed by the rational development of hybrid heterojunction nanocomposites *via* various synthesis strategies for application in the fixation of N_2 to NH_3 . Finally, the review is concluded with a summary, invigorating perspectives and future prospects on this research horizon. As such, it is projected that this article will markedly promote the importance of this research platform and help to provide new insights for the exploration of future investigations toward a sustainable future.

2. Fundamental process of N_2 photoreduction

2.1. Basic photocatalytic principles over semiconductors

The photocatalytic process of N_2 fixation can be divided into several steps. First, the photogenerated electrons are promoted to the conduction band, leaving vacant holes in the valance band. Afterwards, some of the electrons and holes recombine with each other; meanwhile, others migrate to the surface of the catalyst and participate in the redox reaction. Specifically, H_2O can be oxidized to O_2 by the holes, whereas N_2 is reduced to NH_3 after a series of multi-step injections of photogenerated electrons and water-derived protons.

The hydrogenation reactions related to this process and the corresponding reduction potentials are summarized in Table 1.^{68–71} As is known to all, whether the photocatalytic redox reaction can occur largely depends on the reduction potential of the adsorbate and the position of the energy band in the

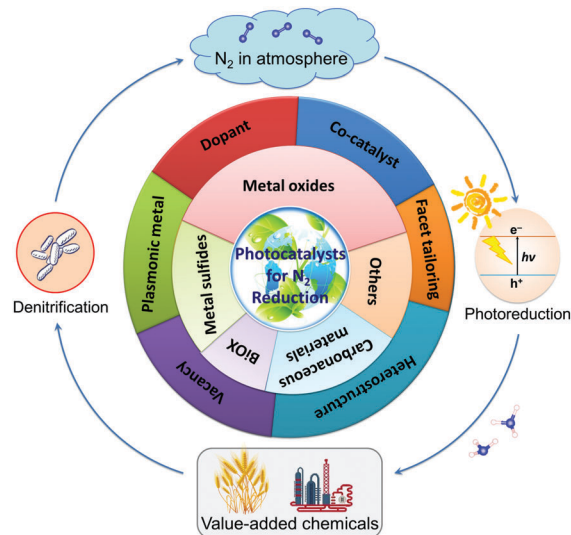


Fig. 1 Illustration of the main topics covered in this review article, exemplifying the latest research in the development of photocatalysts for N_2 reduction.

Table 1 Reduction potentials (vs. NHE at pH 0) of typical hydrogenation reactions related to the reduction of N_2 to NH_3 ^{68–71}

Reaction	E^0 (V)
$H_2O \rightarrow \frac{1}{2}O_2 + 2H^+ + 2e^-$	0.81 ^a
$2H^+ + 2e^- \rightarrow H_2$	−0.42 ^a
$N_2 + e^- \rightarrow N_2^-$	−4.16
$N_2 + H^+ + e^- \rightarrow N_2H$	−3.2
$N_2 + 2H^+ + 2e^- \rightarrow N_2H_2$	−1.10 ^b
$N_2 + 4H^+ + 4e^- \rightarrow N_2H_4$	−0.36
$N_2 + 5H^+ + 4e^- \rightarrow N_2H_5^+$	−0.23
$N_2 + 6H^+ + 6e^- \rightarrow 2NH_3$	0.55
$N_2 + 8H^+ + 8e^- \rightarrow 2NH_4^+$	0.27

^a Reduction potential E^0 vs. NHE at pH 7. ^b Reduction potential E^0 vs. RHE.

semiconductor (Fig. 2).^{72–85} For example, the position of the semiconductor conduction band should be higher (more negative) than the reduction potential of the N_2 hydrogenation, while the valance band should be lower (more positive) than the oxygen evolution potential. The maximum energy transition state is located in the very first electron transfer (−4.16 V vs. NHE) and proton-coupled electron transfer (−3.2 V vs. NHE) processes (Table 1), hampering the overall kinetic reaction.⁸⁶ On this basis, these are the main two limitations that must be overcome to activate N_2 molecules for NH_3 formation. It is of utmost importance to maintain a small band gap of the semiconductor, preferably in the visible light region, which can still satisfy the thermodynamic reduction potentials of N_2 to NH_3 . Additionally, it is necessary to suppress the recombination of charge carriers in semiconductor photocatalysts in order to enhance the solar conversion efficiency and apparent quantum yield (AQY) of the reaction.

2.2. N_2 reduction mechanism

Recently, a number of investigations from the viewpoint of experimental and density functional theory (DFT) calculations

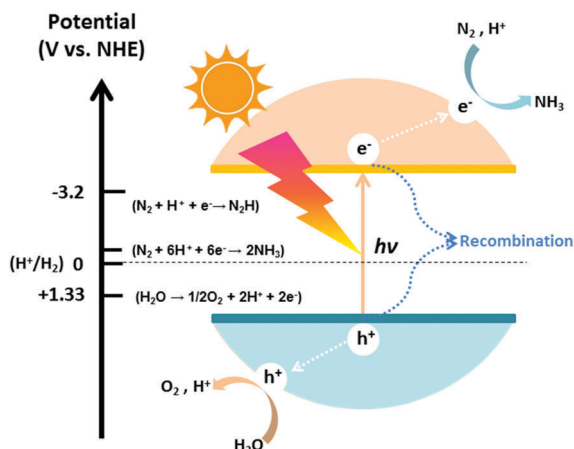


Fig. 2 Schematic of semiconductor-based photocatalysts used for the conversion of N_2 to NH_3 . The redox potentials (V vs. NHE at pH = 0) of water splitting and dinitrogen hydrogenation are marked on the left.

have been carried out to demystify N_2 reduction mechanisms over various catalysts.^{87–89} As is mentioned above, in the case of photo-driven NH_3 synthesis, elementary electrochemical reactions can be employed to help decipher the hydrogenation process in greater detail. For example, at the very first proton-coupled electron transfer, the N_2 adsorbed on the catalyst surface ($\text{*N}\equiv\text{N}$) gains one proton (H^+) from the environment and one photo-generated electron (e^-) from the catalyst to generate an adsorbed chemical species ($\text{*N}=\text{NH}$) as shown: $\text{*N}\equiv\text{N} + \text{H}^+ + \text{e}^- \rightarrow \text{*N}=\text{NH}$.

For the following transfer of H^+/e^- pairs, 5 routes were proposed by Azofra *et al.* in their DFT study (Fig. 3).⁸⁷ There are two widely accepted mechanisms for the conversion of N_2 to NH_3 . These are commonly called distal and alternating mechanisms.¹⁹ In the distal mechanism, H^+/e^- pairs are proposed to consecutively attach to one N atom of N_2 to form a terminal nitride intermediate, liberating the first NH_3 and leaving a single N, which finally converts into another NH_3 (Fig. 3, path 1). In contrast, the alternating mechanism postulates that H^+/e^- pairs occur alternately on the two N atoms of N_2 (Fig. 3, path 2).

In the study of the N_2 fixation mechanism, the combination of experimental investigation with computational simulation will help us to further understand the reaction routes: the computational simulation gives a prospective direction for guidance of further experiments, while the experimental research provides feedback and confirmation of the optimization of the theoretical model.

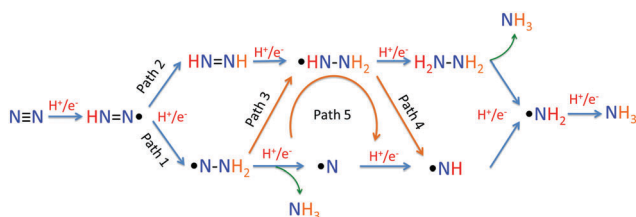


Fig. 3 Five proposed routes for the conversion of N_2 to NH_3 . Reproduced with permission.⁸⁷ Copyright 2016, Royal Society of Chemistry.

3. Classification of photocatalysts for N_2 fixation to NH_3

Most traditional unmodified semiconductors cannot meet the energy standards for the reduction potentials of the intermediate reactions. Hitherto, many concerted efforts have been made regarding the choice and modification of semiconductors, such as doping, introducing vacancies, plasmon induction, facet tailoring and heterostructure assembly, to improve the photocatalytic performance. In the subsequent sections, the photocatalysts are classified based on their elemental compositions.

3.1. Metal oxide-based materials

3.1.1. Titanium oxide-based materials. The excellent performance of the photolysis of water on TiO_2 created great awareness of the application of TiO_2 -based nitrogen photofixation catalysts.⁹⁰ In 1988, Bourgeois and his partners reported that unmodified TiO_2 exhibited N_2 photocatalytic activity after annealing in air because the thermal pretreatment generated surface defects which introduced defect or impurity states in the band gap of the semiconductor.⁹¹ Most recently, the photocatalytic conversion of N_2 to NH_3 on the surface oxygen vacancies of TiO_2 was systematically studied by Shiraishi's group.⁹² Among the tested catalysts, JRC-TiO-6 (rutile phase) exhibited the highest N_2 fixation activity, with a 2.7-fold enhancement using 2-ProH as a sacrificial electron donor for 12 h of reaction. Further research corroborated that the loading of Ru, Pt or Pd particles would not enhance the yield of NH_3 because these particles covered the Ti^{3+} induced by surface oxygen defects. As revealed in Fig. 4a, the superficial Ti^{3+} provided abundant active sites for N_2 fixation by acting as an electron donor, leading to relative ease of dissociation of the $\text{N}\equiv\text{N}$ bond. With several transformations of surficial Ti from Ti^{3+} to Ti^{4+} , the electrons were naturally injected into N_2 . Meanwhile, Ti^{3+} could be regenerated under UV irradiation. The ground-breaking exploration on TiO_2 -based materials dates back to 1977. Schrauzer and Guth synthesized iron-doped TiO_2 by heating iron(III) sulfate-impregnated anatase TiO_2 ; they testified to its great ability to reduce N_2 under UV irradiation.⁶⁷ In their work, ammonia and a small quantity of hydrazine were detected, with the iron content in TiO_2 varying from 0% to 1%. Interestingly, the NH_3 yields reached a maximum value over 0.2% Fe_2O_3 -doped TiO_2 under UV. The facile impregnation method described in this research has thus enlightened and inspired research endeavors by multitudinous worldwide researchers.

After that, Augugliaro *et al.* utilized an identical impregnation technique to prepare Fe_2O_3 -hybridized TiO_2 and supported it on Al_2O_3 . An improved NH_3 production rate was gained in gas-solid fluidized bed reactors.⁹³ According to literature reports, the effect of iron ions facilitated the transformation of the crystallinity of TiO_2 , which noticeably affected the photocatalytic efficiency. Notably, the incorporation of Fe accelerated the phase transformation of anatase into rutile and also promoted grain growth during calcination. In this regard, the ratio of anatase to rutile played a prevailing role in the efficiency of the catalysts by maintaining a constant concentration of iron.^{94,95} After a prolonged calcination process, the increased content and growing grain size of rutile

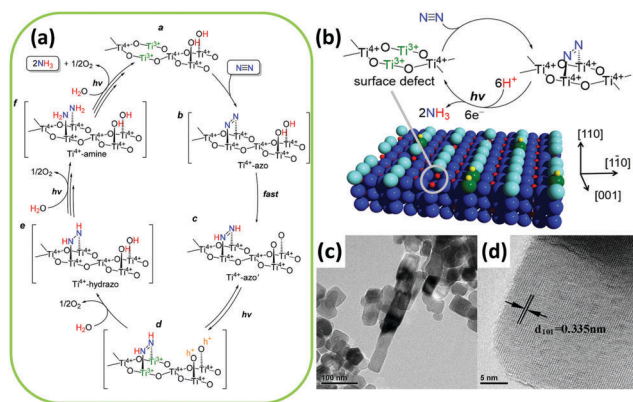


Fig. 4 (a) Mechanism for N_2 conversion to NH_3 over the surface oxygen vacancies of TiO_2 . (b) A photocatalytic cycle for N_2 reduction at the surface of rutile $TiO_2(110)$. Reproduced with permission.⁹² Copyright 2017, American Chemical Society. (c) Transmission electron microscopy (TEM) and (d) high-resolution TEM (HRTEM) images of Fe^{3+} -doped TiO_2 . Reproduced with permission.⁹⁹ Copyright 2014, Elsevier.

phase as well as the loss of surface $Ti-OH$ groups led to a decrease of the active surface area, resulting in inferior photocatalytic performance.⁶⁷

Several authors have employed diversified methods in the preparation of iron-doped TiO_2 . In Radford and Francis's research, both the anatase and rutile phase of TiO_2 were sampled for doping with iron in metal vapor without high-heat treatment.⁹⁶ Aqueous suspensions of samples were irradiated under UV light. Undoped samples demonstrated minimal or no activity under light irradiation. It should be noted that the activity of doped anatase was higher than that of doped rutile, which can be attributed to the more negative flat band potential of anatase.⁹⁷ The author investigated whether iron was the sole active species involved in the photoactivity because the yield of ammonia over iron-doped anatase was far beyond their anticipation. However, Schrauzer indicated later that the NH_3 may have formed on a photo-assisted organoiron compound.⁶⁶ As for the role of Fe^{3+} , Soria *et al.* demonstrated that iron ions could temporarily trap photogenerated electrons and promote the separation of charge carriers.⁹⁸ They coprecipitated an aqueous solution of $TiCl_3$, which contained Fe^{3+} ions, in an ammonia solution; they then heated the resulting solid for a day. The residual chloride ions were noted to exhibit poor activity of the coprecipitation specimens. Recently, Fe-doped TiO_2 with highly exposed (101) facets obtained *via* a hydrothermal method by adsorbing Fe^{3+} on a precursor of hydrogen titanate nanotubes was reported by Zhao *et al.* (Fig. 4c and d).⁹⁹ The N_2 photoreduction performance was enhanced by exposing the (101) facets of Fe-doped TiO_2 with ethanol as the scavenger. A low doping concentration of Fe^{3+} on the TiO_2 surface enhanced the trapping of electrons and holes by forming Fe^{2+} and Fe^{4+} to inhibit charge recombination. The unstable Fe^{2+} and Fe^{4+} transferred electrons and holes to Ti^{4+} and OH^- , generating Ti^{3+} (as mentioned in the preceding section, Ti^{3+} plays an essential role in the photocatalytic activation)⁹² and $\bullet OH$, respectively. Similar to the findings by Soria *et al.*,⁹⁸ the authors mentioned that no nitrite was formed in the presence of

ethanol solution because ethanol functioned as a scavenger of $\bullet OH$ to prevent the oxidation of ammonia.

Apart from iron-doped TiO_2 , other transition metals have been used as dopants in TiO_2 .^{100–103} The reports of these investigations, while significant, were popular in the last century; however, they are receiving little attention at present because there have been few breakthroughs in their activity in N_2 photoreduction.^{100,101} In the original study, Schrauzer and Guth tested eleven metal dopants in addition to iron, including Co, Mo, Ni, Pd, V, Cr, Cu and the noble metals Pt, Ag, Au, and Pb.⁶⁷ Compared to the control group, the Co, Mo and Ni dopants contributed to enhancement of the NH_3 yield of TiO_2 . However, eight other metals presented inhibitive effects on NH_3 formation. This phenomenon was attributed to the different influences of the metal dopants on the phase transformation of TiO_2 . Apparently, the samples containing Co, Mo and Ni accelerated the anatase to rutile transformation during heat treatment; meanwhile, no acceleration of phase transformation was readily observed on doping with eight other metals. In contrast, a different phenomenon was manifested by Palmisano and his co-workers, where chromium-ion-doped TiO_2 was found to be effective in N_2 photoreduction.¹⁰⁰ They clarified that compared with iron-ion-doped TiO_2 , the chromium-ion-doped TiO_2 demonstrated shorter diffusion lengths of minority carriers, accounting for its higher rate of hole–electron recombination. Another study suggested that chromium ions were mainly dispersed on the surface in the formation of the solid solution. The increase of Cr ions reduced the OH groups on the surface, which explains its lower activity at higher contents.¹⁰¹ Dopants such as Mg, Ce and V have also been investigated in TiO_2 -based photocatalysts by Ileperuma *et al.*^{102,103} In their work, catalysts were suspended in double-distilled water under irradiation. The results implied that the ammonia yield increased with increasing pH value. At the same time, higher nitrate content was detected in production.¹⁰² Similar studies involved doping TiO_2 with a relatively high concentration of 10 wt% Ce or V. The V-doped TiO_2 catalysts were shown to possess n-type semiconductor behavior at pH = 3, while the Ce-doped TiO_2 catalysts displayed p-type behaviour at pH = 12.5.¹⁰³ However, there was no substantial difference in the NH_3 yields of both systems.

In addition to the modification of metal doping, transition metals can also be loaded on the TiO_2 surface as a co-catalyst. For example, Miyami *et al.* have reported the enhancement of N_2 photoreduction using Ru-loaded TiO_2 .¹⁰⁴ Khan *et al.* used a Ru(III) complex as a photosensitizer in a Pt- TiO_2 semiconductor.¹⁰⁵ Ru(III) complex could be excited and subsequently inject electrons into the conduction band of TiO_2 to form a Ru(IV) complex. A systematic study on noble metal-loaded TiO_2 was investigated by Ranjit *et al.*¹⁰⁶ By comparing four noble metal catalysts as co-catalysts of TiO_2 , they found the order of photoactivity was $Ru > Rh > Pd > Pt$, which is closely associated with the strength of the M–H bond (M = noble metal). In other words, the incorporation of noble metals, which exhibit a high barrier for H_2 evolution, resulted in high NH_3 yields. In 2008, Linnik and Kisch designed a Ru-modified TiO_2 film with conducting glass as the substrate and humic acid as the sacrificial agent.¹⁰⁷

However, the activity of the catalysts was not greatly improved compared to other doping systems.

In 2000, Hoshino *et al.* designed a TiO₂/conducting polymer system with an organic/inorganic heterojunction.¹⁰⁸ The photo-generated carriers at the organic/inorganic interface led to the synthesis of ammonia. In their work, a composite of poly(3-methylthiophene) (P3MeT) and TiO₂ was irradiated under a fluorescent lamp, and NH₄⁺ClO₄[−] needle crystals were obtained. A rigorous comparison with Schrauzer's method was performed in the following year, and a comparable ammonia production rate was obtained.¹⁰⁹ It was deduced that the separation of photogenerated charge carriers at the interface and the presence of P3MeT inhibited the accumulation of NH₃ in TiO_x. A further study was conducted by substituting TiO₂ crystal with its amorphous phase in 2007.¹¹⁰ These investigations undoubtedly provide a new concept and future direction of catalyst modification.

3.1.2. Other binary metal oxides. Many unremitting efforts have been devoted to the study of other metal oxides, such as iron oxide,^{111–113} tungsten oxide,¹¹⁴ gallium oxide and bismuth monoxide.^{115,116} Recent achievements have provided unprecedented ideas and vistas for investigations toward the application of metal oxides in N₂ photoreduction.

Most earlier studies suggested that bare Fe₂O₃ has no photocatalytic activity for N₂ cleavage.^{67,98,117} It is worth noting that iron is useful in the Haber–Bosch process and also functions similarly to a nitrogen enzyme because of its good interaction with dinitrogen.^{6,19,112} As expected, later studies have proven that ferric oxide is capable of photofixating nitrogen to ammonia.^{111,113} However, in a pure form, neither Fe₂O₃ nor its reduced product Fe₃O₄ had N₂ photocatalytic activity. To overcome this bottleneck, Khader *et al.* successfully designed α -Fe₂O₃, which was effective in photo-activating nitrogen by partially reducing α -Fe₂O₃ to Fe₃O₄.¹¹¹ Fascinatingly, in the presence of 3 to 5 at% iron in the form of Fe(II) in the partially reduced Fe₂O₃, NH₃ was detected in an aqueous slurry of the catalyst under UV irradiation. Most recently, another comparison of Fe₂O₃ and TiO₂ was performed by Lashgari and Zeinalkhani.¹¹³ The 1:1 ratio nanocomposites of Fe₂O₃–TiO₂ and Pd-loaded Fe₂O₃–TiO₂ were taken into consideration. It is noteworthy that the rate of NH₃ production was in the order of TiO₂ < Fe₂O₃–TiO₂ < Pd/Fe₂O₃–TiO₂. Therefore, with the incorporation of Fe₂O₃ into TiO₂, the coupled heterojunction nanocomposites played a profound role in the N₂ photoreduction process owing to the extended photoabsorption of visible light in Fe₂O₃.

Furthermore, tungsten oxide with oxygen vacancies (WO_{3–x}) was reported to have poor activity in the gas phase.¹¹⁴ ZnO was reported to have photocatalytic activity for nitrogen fixation.¹¹⁸ In the case of commercial ZnO, the ammonia yield of unmodified ZnO was greater than that of Pt-loaded ZnO, which is consistent with a previous report by Miyama in 1980.¹⁰⁴ However, for ZnO prepared by means of wet etching or precipitation methods (Fig. 5a and b), the situation was reversed. For a wide band gap semiconductor, mesoporous β -Ga₂O₃ nanorods were employed in N₂ photoreduction by Zhao *et al.* in 2015.¹¹⁵ The photoactivity of β -Ga₂O₃ was ameliorated in the presence of different alcohols, including methanol, ethanol, and *tert*-butanol (TBA), which

formed $\bullet\text{CO}_2^-$ *in situ*. The reducing ability of $\bullet\text{CO}_2^-$ dramatically enhanced the reduction of N₂ to NH₃. Moreover, the presence of O₂ in the N₂ facilitated the formation of $\bullet\text{CO}_2^-$, which enhanced the reducing power (Fig. 5c). Very recently, a low-valent bismuth monoxide (BiO) without additional reducing agents was employed for N₂ photoreduction because the low-valent bismuth with empty 6d orbitals provided excellent N₂ chemisorption and activation centres (the synthesis procedure is shown in Fig. 5d). The N₂ was activated by three arranged Bi atoms by donating electrons to the 6d orbitals of Bi and accepting lone pairs of electrons from the three Bi atoms to its anti-bonding orbitals (σ^*2p_x , π^*2p_y and π^*2p_z) (Fig. 3e).¹¹⁶

In addition to the above-discussed TiO₂ photocatalyst, as reported in Section 3.1.1., ferric oxide has been shown to be a compelling and effective photocatalyst for N₂ photoreduction. Importantly, the narrow band gap of Fe₂O₃ guarantees its photocatalytic activity even in the visible light region.¹¹⁹ Although semiconductors with wide band gaps are favorable in the activation of N₂ as a result of their high redox abilities, they remain limited in their UV response. It is worth mentioning that bismuth-containing systems may be useful in N₂ fixation; this will be further corroborated in Section 3.3.

3.1.3. Ternary metal oxides. The development of iron-doped TiO₂ in N₂ photoreduction has invigorated interest in ternary metal oxides, such as iron titanate. At a high concentration of Fe, the excess Fe³⁺ will form pseudobrookite (Fe₂TiO₅) phase. This multiphasic compound was shown to have no photocatalytic activity.^{117,120} Soria *et al.* also indicated that no NH₃ production was detected over pure Fe₂TiO₅ synthesized by a coprecipitation method.⁹⁸

However, there are some controversial opinions on the possible use of iron titanate in N₂ fixation, as reported in 2001.¹²¹ The dominant hypothesis for the conflicting results in Fe systems is mainly accredited to the different approaches to catalyst preparation.¹²² Using the sol–gel method, Rusina

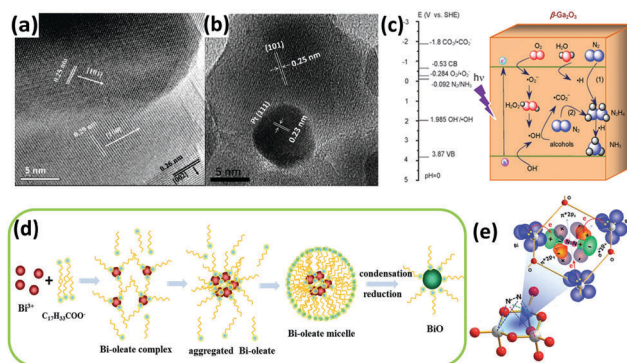


Fig. 5 HRTEM images of (a) the fusion of three prominent lattice planes along the wet etching ZnO grain boundaries and (b) a Pt cluster at the grain boundary. Reproduced with permission.¹¹⁸ Copyright 2010, American Chemical Society. (c) Possible electron transfer pathways for the conversion of N₂ to NH₃ over β -Ga₂O₃. Reproduced with permission.¹¹⁵ Copyright 2015, Royal Society of Chemistry. (d) Schematic of the synthesis process for BiO quantum dots. (e) A 1N₂–3Bi(II) side-on bond structure formed by electron sharing. Reproduced with permission.¹¹⁶ Copyright 2017, Royal Society of Chemistry.

and his coworkers prepared iron titanate films with relatively high Fe contents by reacting iron chloride and tetraisopropyl titanate, leading to the successful development of a new $\text{Fe}_2\text{Ti}_2\text{O}_7$ phase.¹²¹ After 90 min of light irradiation ($\lambda \geq 320$ nm), a maximum ammonia yield of 17 μM was obtained at 75% alcohol content when Fe/Ti was fixed at 1:1. The produced ammonia was subsequently oxidized to nitrite in the presence of ethanol. Meanwhile, in another report, Zhao *et al.* revealed that ethanol could prevent the oxidation of ammonia.⁹⁹ In a continuation of their work, further investigations on iron titanate films were conducted by Kisch and Linnik.¹²³ The electron transfer mechanism of N_2 fixation on the $\text{Fe}_2\text{Ti}_2\text{O}_7$ thin films involved a series of photochemical processes of nitrogen \rightarrow diazene \rightarrow hydrazine \rightarrow ammonia \rightarrow nitrate. In addition, the essential role of chloride ions was discussed. Although Schrauzer and Soria have noted that the generation of TiO_2 using chloride ions is unfavorable,^{98,124} both the inhibiting and accelerating effects of iron chloride as the precursor were corroborated.

In addition to iron titanate systems, titanate-like SrTiO_3 and BaTiO_3 have also been investigated under UV irradiation for N_2 photoreduction. Judging from the results of the experiments, undoped SrTiO_3 and BaTiO_3 produced minimal NH_3 yields (0.82 and 1.74 $\mu\text{mol g}_{\text{cat}}^{-1}$ after 2 h of reaction, respectively). Their yields of NH_3 reached 5 to 5.2 $\mu\text{mol g}_{\text{cat}}^{-1}$ in 2 h when doped with RuO_2 and NiO .¹²⁵ In another paper, plasmonic-metal/semiconductor photocatalysts elicited great attention for their high light-harvesting properties.¹²⁶ Using gold nanoparticles (Au-NPs) as the plasmonic nanostructure, Oshikiri and his co-workers designed Au-NPs/ Nb-SrTiO_3 /Ru (Fig. 6a) and Au-NPs/ Nb-SrTiO_3 /Zr/ ZrO_x (Fig. 6b–d) semiconductor photoelectrodes in

2014 and 2016, respectively.^{127,128} Au-NPs were loaded on a 0.05 wt% niobium-doped strontium titanate (Nb-SrTiO_3) single crystalline substrate, and Ru or Zr film as a co-catalyst was deposited on the opposite side of Nb-SrTiO_3 (Fig. 6c and d). Zr was oxidized to ZrO_x . Ethanol was added as a sacrificial electron donor in the anodic chamber. In later reports, the production rates of Zr/ ZrO_x and Ru systems were compared to evaluate the production selectivity. Interestingly, H_2 was the main product in the case of Ru systems, indicating that proton reduction is the primary reaction on the Ru co-catalyst. In contrast, in the case of Au-NPs/ Nb-SrTiO_3 /Zr/ ZrO_x , the production rate of NH_3 was conspicuously higher because Zr and ZrO_x bind N more favorably than H.¹²⁹ However, its NH_3 production rate was still obviously lower than that of the electrosynthesis of ammonia.¹³⁰ Recently, sparked by the unique features of Mo element in the Mo-cofactor of nitrogenase enzymes, Hao *et al.* fabricated hydrogenated bismuth molybdate ($\text{H-Bi}_2\text{MoO}_6$) which was capable of reducing N_2 under sunlight.¹³¹ In this context, the hydrogenation reaction induced oxygen vacancies on Bi_2MoO_6 (Fig. 6e–h), endowing $\text{H-Bi}_2\text{MoO}_6$ with activity under visible light for N_2 fixation. Using air instead of pure nitrogen, the NH_3 production rate under sunlight was as high as 1.3 $\text{mmol g}^{-1} \text{h}^{-1}$. This high nitrogen activation could not be attained if molybdenum was replaced with tungsten as a counterpart or if the hydrogenation process was omitted.

Judging from the existing literature, we can conclude that most of the investigations of ternary metal oxides are focused on titanate systems.^{121–123,125,127,128} Iron titanate exhibits relatively high photoactivity in N_2 fixation under UV irradiation, in a pure nitrogen flow, and in the presence of organic scavengers. On the other hand, bismuth molybdate has been reported to enable impressive NH_3 production rates after performing the hydrogenation process under mild conditions. However, for N_2 activation, strontium titanate does not reach the general level of other catalysts even after modification by doping or plasmon induction.

3.1.4. Hydrous oxides. As early as 1987, Tennakone and his co-workers discovered hydrous ferric oxide photocatalysts for N_2 reduction under visible light.¹³² They attested that hydrous ferric oxide was superior to TiO_2 in the case of N_2 fixation because of its exceptional nitrogen chemisorption and highly negative flat band potential.¹³³ Since then, hydrous oxides such as $\text{Cu}_2\text{O} \cdot x\text{H}_2\text{O}$,¹³⁴ $\text{Sm}_2\text{O}_3 \cdot x\text{H}_2\text{O}$ / $\text{V}_2\text{O}_3 \cdot x\text{H}_2\text{O}$ and $\text{WO}_3 \cdot \text{H}_2\text{O}$ have been systematically investigated as photocatalysts for N_2 reduction.^{135,136}

In the initial study by Tennakone *et al.*, amorphous Fe_2O_3 (H_2O)_n was prepared by gradually adding KOH solution to FeCl_3 solution. After saturation with N_2 , the solution was irradiated under a 100 W tungsten lamp (IR and UV filtered off). A maximum NH_3 yield of ca. 4 μM was detected after 40 min.¹³² In 1991, ultrafine particles of $\text{Fe}(\text{O})\text{OH}$ were prepared from photohydrolysis of iron(II) bicarbonate by the same author. Nitrate was also detected in the solution after prolonged irradiation. The initial quantum yield of NH_3 was about 10^{-2} , which is higher than that of hydrous ferric oxide ($\sim 10^{-3}$).¹³³ Ilerperuma *et al.* claimed that a hydrous ferric oxide-loaded

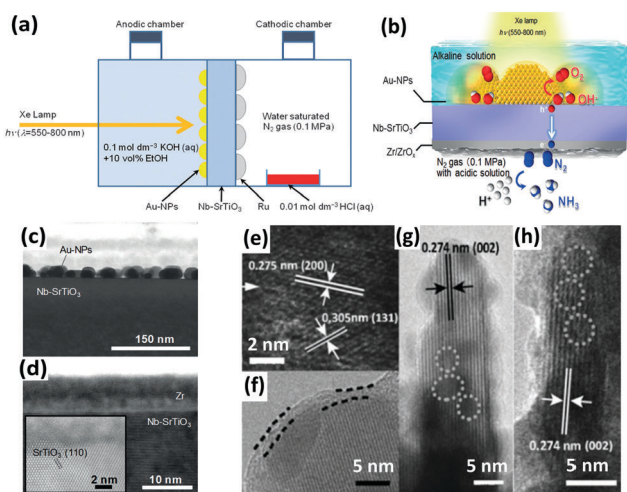


Fig. 6 (a) Schematic of the NH_3 photosynthesis device using an Au-NPs/ SrTiO_3 photoelectrode. Reproduced with permission.¹²⁷ Copyright 2014, Wiley-VCH. (b) Diagram of NH_3 synthesis on the Au-NPs/ Nb-SrTiO_3 /Zr/ ZrO_x photoelectrode. Cross-sectional view of the bright field scanning TEM (BF-STEM) images of (c) the Au-NPs/ Nb-SrTiO_3 interface and (d) the Zr film deposited onto Nb-SrTiO_3 . Reproduced with permission.¹²⁸ Copyright 2016, Wiley-VCH. (e–h) HRTEM images of $\text{H-Bi}_2\text{MoO}_6$ (the superficial and lattice disorders induced by defects are marked by parallel dashed lines and circles, respectively). Reproduced with permission.¹³¹ Copyright 2016, Wiley-VCH.

bentonite system produced more NH_3 and less nitrate than the parent hydrous ferric oxide under UV irradiation.¹³⁷ In contrast with pure hydrous ferric oxide, a system of coprecipitating Fe(III) and Ti(IV) hydrous oxides (Ti to Fe ratio = ~8%) was found to be more effective in the generation of NH_3 , while the rate of nitrate production using this composite was comparatively low.¹³⁸ Hydrous ferric oxide was believed to play roles in nitrogen chemisorption and reduction, while TiO_2 provided hole accumulation centres. Although the authors revealed the predominant effect of the heterojunction interface in the mechanism of electron-hole separation, they still questioned the meaning of these concepts in a colloidal system. In 1992, the yield of vanadium-substituted hydrous ferric oxides was ameliorated under UV irradiation. V^{3+} sites demonstrated distinctive attributes in capturing photo-generated holes in the mixed hydroxide.¹³⁹ With the incorporation of V^{3+} , a maximum NH_3 yield of about 200 μM was reached in about 24 h when the vanadium-to-iron ratio was at unity. The subsequent decrease of NH_3 concentration was ascribed to the inactivation of catalyst followed by the photocatalytic decomposition of NH_3 . This reason for the decrease of ammonia was also suggested in 1987 because of the continuous generation of H_2 and the unchanged content of O_2 .¹³² Conversely, Ieperuma *et al.* pointed out that NH_3 was oxidized to nitrate because NO_2^- and NO_3^- were detected in the final products along with a decrease in NH_3 yield.¹³⁷

Additionally, hydrous cuprous oxide was able to photoreduce N_2 to NH_3 after impregnation with cuprous chloride, which underwent sacrificial oxidation to form cupric chloride. The high ammonia yield presumably resulted from the separation of oxidation and reduction sites as well as the chemisorption of N_2 on $\text{Cu}_2\text{O} \cdot x\text{H}_2\text{O}$, which served as reduction sites.¹³⁴ Pursuing the exciting idea in a previous study of coprecipitated hydrous oxides of Fe and Ti,¹³⁸ a coprecipitate of samarium(III) and vanadium(III) was subsequently explored.¹³⁵ The maximum NH_3 yield was obtained within 1 h when the V-to-Sm ratio was ~1. When employing this composite, the ammonia production rate was strikingly higher than that of previously reported vanadium-substituted hydrous ferric oxide.¹³⁹ Very recently, highly efficient N_2 photoreduction was achieved over carbon- $\text{WO}_3 \cdot \text{H}_2\text{O}$ (HWO-C) in water.¹³⁶ $\text{WO}_3 \cdot \text{H}_2\text{O}$ was selected as the photocatalyst due to its extraordinary electron and proton conductivity. As a result, the rapid transfer of photogenerated electrons and water-derived protons to N_2 was enhanced. In this circumstance, carbon modification prominently enhanced the NH_3 production rate of HWO by increasing its surface activation and simultaneously promoting the separation and transport of charge carriers to retard the electron-hole recombination rate. A similar phenomenon in the use of other carbon-modified photocatalysts for potential energy applications has also been reported by our research group.¹⁴⁰ Therefore, it is evident that the modification of carbon plays a decisive role in suppressing the recombination of electron-hole pairs by prolonging the lifetime of charge carriers for enhanced photoactivity.

3.2. Metal sulfide-based materials

In addition to the large family of metal oxide-based photocatalysts, the exploration of metal sulfides has also experienced a

tremendous upsurge in the scientific community, especially in the field of photocatalysis.^{141–143} The narrow band gap of metal sulfides is conducive to strong absorption of visible light, which results in highly efficient solar utilization efficiency.

In 1980, Miyama *et al.* employed CdS semiconductors for the fixation of nitrogen under UV irradiation; the recorded yield of NH_3 in 5 h was 10.67 $\mu\text{mol g}_{\text{cat}}^{-1}$.¹⁰⁴ They constructed CdS/Pt binary wafered catalysts whose NH_3 yield was drastically higher than that of pristine CdS. The remarkable performance of the loading of Pt co-catalysts has heightened research interest in other potential modifications of CdS photocatalysts. In 1988, Khan *et al.* reported the fixation of N_2 with a CdS/Pt/ RuO_2 semiconductor particulate system under the illumination of visible light ($\lambda = 505 \text{ nm}$).¹⁴⁴ Dinitrogen was activated to react with $[\text{Ru}(\text{Hedta})\text{H}_2\text{O}]^-$ to form the Ru(II) dinitrogen complex. The holes in the valence band trapped the electrons released from RuO_2 . Two years later, a similar research team conducted the stepwise reduction of dinitrogen to ammonia on visible-light-responsive Pt/CdS- $\text{Ag}_2\text{S}/\text{RuO}_2$ photocatalysts.¹⁴⁵ The addition of silver facilitated the migration of electrons from the conduction band to minimize the photocorrosion of CdS. The production rate of NH_3 was twice that in the absence of silver. In view of the obtained results, it is clear that noble metals such as Pt, Ag and Ru work well with CdS. The decrease in the yield of NH_3 over time may originate from the photocorrosion of CdS to S and Cd^{2+} .¹⁴⁴ To retain the high photocatalytic activity and stability of CdS for the reduction of N_2 to NH_3 , in 2017, Ye *et al.* demonstrated the fixation of N_2 using $\text{Cd}_{0.5}\text{Zn}_{0.5}\text{S}$ solid solution for the first time.¹⁴⁶ To enhance the photocatalytic performance, a transition metal phosphide (Ni_2P) was employed as a co-catalyst to rapidly transfer the photoinduced electrons to Ni_2P via well-contacted heterointerfaces to diminish the charge recombination.

On the other hand, owing to the recent interdisciplinary interest in material science and biology, organic-sulfide catalysts have also been designed for enhanced N_2 fixation activity. In 2016, Brown *et al.* reported nitrogen reduction by the MoFe protein, which is the active site of nitrogenase, adsorbed onto CdS nanorods to form biohybrid complexes.¹⁴⁷ The NH_3 production rate reached 315 nmol per mg MoFe protein per min under visible light. In this regard, CdS nanocrystals were used to photosensitize the MoFe protein so that the photon energy was derived from ATP (Fig. 7a). Furthermore, the rates were comparable to that of physiological NH_3 production by nitrogenase with energy provided by ATP. Because the active sites of nitrogenase contain the elements Fe, Mo and S, a synthetic complex of Fe, Mo and S could be taken into account. By exploiting the advantage of the FeMo cofactor in nitrogenases, Banerjee *et al.* inferred that biomimetic chalcogels comprising FeMoS inorganic clusters could reduce N_2 to NH_3 in aqueous media under light.¹⁴⁸ The $\text{Fe}_2\text{Mo}_6\text{S}_8$ chalcogel was an analog to the MoFe active site in the enzyme and was linked by Sn_2S_6 ligands to form an amorphous network (Fig. 7b). This study proved that structural analogues of nitrogenase can be functional and can even confer better properties than nitrogenase. In 2016, to make a better mimic of nitrogenases, not only MoFe protein but also Fe protein was considered by Liu *et al.*¹⁴⁹ They employed

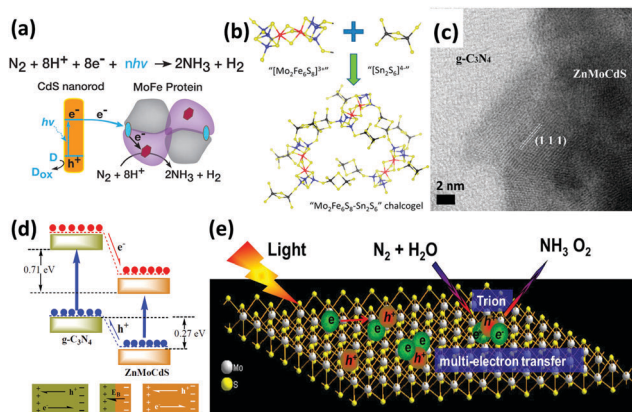


Fig. 7 (a) Reaction scheme for N_2 reduction to NH_3 by CdS:MoFe protein biohybrids. Reproduced with permission.¹⁴⁷ Copyright 2016, American Association for the Advancement of Science. (b) Schematic of the composition of $Mo_2Fe_6S_8-Sn_2S_6$ biomimetic chalcogel. Reproduced with permission.¹⁴⁸ Copyright 2015, American Chemical Society. (c) HRTEM image of $g-C_3N_4/ZnMoCdS$. (d) Schematic of the charge transfer process at the heterojunction interface of $g-C_3N_4/ZnMoCdS$. Reproduced with permission.¹⁵⁵ Copyright 2016, Royal Society of Chemistry. (e) Schematic of the trion-induced multi-electron N_2 reduction process. Reproduced with permission.⁷¹ Copyright 2017, Elsevier.

a chalcogel system consisting of $Fe_2Mo_6S_8(SPh)_3$ and Fe_3S_4 biomimetic clusters linked by Sn_2S_6 . Iron was believed to be more vital than molybdenum for the light-driven reduction of nitrogen due to the fact that a weak bonding orbital between nitrogen and iron was manifested through localized orbital analysis. More importantly, their conclusion that iron is a better active site for N_2 binding than Mo has also been revealed by recent biochemical and spectroscopic data.^{19,150}

Motivated by the successful fixation of N_2 under visible light with oxygen vacancies on the surface of BiOBr,¹⁵¹ a number of researchers wondered if sulfur vacancies could eventually promote photoactivity. Inspired by this idea, Hu *et al.* obtained $Zn_{0.1}Sn_{0.1}Cd_{0.8}S$ with sulfur vacancies formed by multi-component metal sulfides as catalysts for reducing N_2 under visible light.¹⁵² Surprisingly, the sulfur vacancies introduced chemical adsorption sites on the surface, which aided the activation of N_2 molecules by extending the bond distance between the nitrogen atoms in N_2 . It was also implied that the generation rate of NH_3 was linearly related to the concentration of sulfur vacancies. Additionally, the sulfur vacancies also trapped electrons, thus promoting the separation of photo-induced electrons and holes. In the same year, a similar quaternary system of $Mo_{0.1}Ni_{0.1}Cd_{0.8}S$, which contributed to the reduction of N_2 under visible light, was published by Cao *et al.*¹⁵³ At the same time, tri-component metal sulfides were studied by this group. Two similar heterostructures of $g-C_3N_4/ZnSnCdS$ and $g-C_3N_4/ZnMoCdS$ were employed for N_2 photo-reduction.^{154,155} In the hybrid of $g-C_3N_4/ZnMoCdS$ (Fig. 7c), a tight heterojunction coupling between $g-C_3N_4$ and $ZnMoCdS$ was pivotal for efficient charge transfer. The photogenerated electrons were transferred from $g-C_3N_4$ to the metal sulfide, while the holes were transported in the opposite direction (Fig. 7d).¹⁵⁵

This clearly accounted for the improved visible light absorption after hybridization. Furthermore, the redistribution of electrons and holes on each side of the heterojunction established an internal electric field to impede the recombination of charge carriers.

As a transition metal dichalcogenide (TMD), it is well-known that MoS_2 possesses excellent electrical,¹⁵⁶ optical,¹⁵⁷ and optoelectronic properties.¹⁵⁸ In 2017, Sun *et al.* reported photocatalytic N_2 reduction to NH_3 with ultrathin MoS_2 .¹⁵⁹ In this paper, the photocatalytic performances of MoS_2 samples under different preparation conditions were studied; it was found that the sonicated ultrathin MoS_2 sample generated a large amount of NH_3 with favorably high stability. In ultrathin TMDs, the tightly bound excitons could facilitate capture additional electrons to form charged excitons with more than two electrons in one bound state.¹⁶⁰ Thus, it is believed that these charged excitons functioned as electron-rich species to facilitate the multi-electron reduction process of molecular N_2 (Fig. 7e). Particularly, a six-electron transfer process was responsible for the acceleration of photocatalytic N_2 reduction to NH_3 .

3.3. Bismuth oxyhalides

Bismuth oxyhalides, BiOX (X = Cl, Br, and I), have recently become well known for their superior optical properties; they are also propitious for industrial applications, namely the photodecomposition of organic pollutants.¹⁶¹ The layered structure of BiOX provides adequate space for the polarization of atoms, and the as-formed internal electric field will contribute to the efficient separation and transfer of charge carriers.^{162,163}

In recent years, BiOX has also been reported for applications in solar nitrogen fixation.^{61,86,88,151,164} In 2015, Li *et al.* employed {001}-faceted BiOBr nanosheets with oxygen vacancies (OVs) to reduce N_2 under visible light.¹⁵¹ In this scenario, the N_2 fixation rate was estimated to be $104.2 \mu mol h^{-1}$ (per gram of BOB-001-OV). Remarkably, it was a quantum leap for N_2 fixation under visible light in the absence of organic scavengers. Theoretical simulations revealed that the OVs of BiOBr could elongate the $N \equiv N$ triple bond of adsorbed N_2 from 1.078 to 1.133 Å (Fig. 8a), which subsequently promoted the activation of N_2 molecules. Moreover, the large number of OVs on the surface of BiOBr formed a defect state lying near the bottom of the conduction band of the photocatalyst, hampering the recombination of electron-hole pairs. However, the surface OVs of BiOBr are naturally oxidized, leading to reduced activity. Li's group also examined the photocatalytic activity of BiOCl with OVs on different facets.⁸⁸ They claimed that the kinetics and mechanism of N_2 fixation varied due to the dissimilar facets of BiOCl nanosheets. They highlighted that nitrogen fixation with OVs on the {001} facets followed a distal pathway ($N_2 \rightarrow N-NH_3 \rightarrow N + NH_3 \rightarrow 2NH_3$), whereas the reaction on the {010} facets followed an alternative pathway ($N_2 \rightarrow N_2H_3 \rightarrow N_2H_4$) (Fig. 8b). The quantum yields were $1.8\% h^{-1}$ and $4.3\% h^{-1}$ for OVs on the {001} and {010} facets of BiOCl, respectively, under UV light ($\lambda = 254$ nm). In the most recent work by Ye's group, ultrafine light-switchable OVs of Bi_5O_7Br nanotubes with a diameter of ca. 5 nm and large exposed surface sites were synthesized *via* a water-assisted low-temperature wet chemical approach (Fig. 8c-e).¹⁶⁴

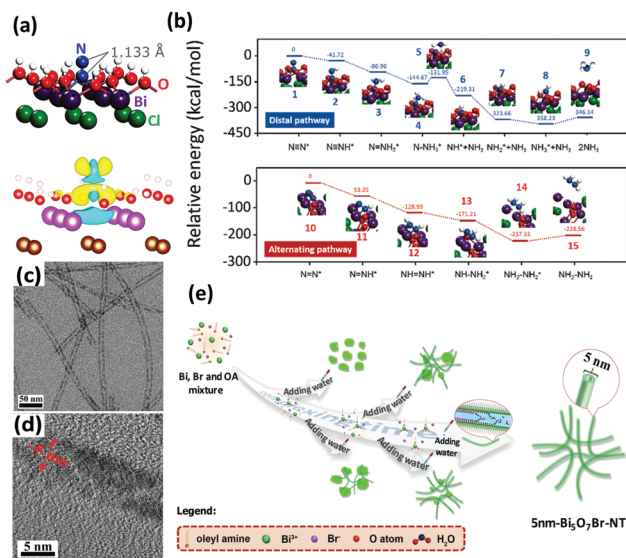


Fig. 8 (a) The adsorption geometry and the charge density difference of N₂ on the OV of the BiOBr (001) surface (the yellow and blue isosurfaces represent charge accumulation and depletion, respectively). Reproduced with permission.¹⁵¹ Copyright 2015, American Chemical Society. (b) Free energy profiles of OV-mediated N₂ fixation on the (001) and (010) surfaces of BiOCl. Reproduced with permission.⁸⁸ Copyright 2016, Royal Society of Chemistry. (c and d) TEM images of Bi₅O₇Br nanotubes at different magnifications. (e) Schematic of the synthesis procedure of ultrafine Bi₅O₇Br nanotubes. Reproduced with permission.¹⁶⁴ Copyright 2017, Wiley-VCH.

The NH₃ generation rate of nanotubes (1.38 mmol h⁻¹ g⁻¹) was 2.5 times higher than that of nanosheets, with an apparent quantum efficiency (AQE) as high as 2.3% at 420 nm.

As a continuation of the previous research by Zhang's and Ye's groups,^{88,164} Bai *et al.* utilized bismuth-rich bismuth oxyhalide (Bi₅O₇I) nanosheets with different dominant {001} and {101} facets.⁸⁹ The N₂ fixation rates of Bi₅O₇I-001 and Bi₅O₇I-100 were 111.5 μmol L⁻¹ h⁻¹ and 47.6 μmol L⁻¹ h⁻¹, respectively. After 5 cycles, the photocatalytic properties and structures of Bi₅O₇I-001 and Bi₅O₇I-100 elucidated high stabilities for the N₂ fixation process. The more negative conduction band potential of Bi₅O₇I-001 (-1.45 V) compared to that of Bi₅O₇I-100 (-0.85 V), explains the higher NH₃ production rate of Bi₅O₇I-001. In short, although most literature studies place significant emphasis on the exposure of different facets, it is conceivable that the combined effects of OVs and facet-dependent studies will open a new outlook and provide inspiration for the development of advanced photocatalysts for N₂ photoreduction. Additionally, the combination of experimental results and theoretical simulations is highly necessary to fully elucidate the mechanism of N≡N triple bond activation and the NH₃ formation pathway. Thus, more emphasis on facet-controlled and vacancy-mediated bismuth oxyhalides should be devoted in the future to accentuate the scientific aspects and unravel the exact reaction steps for N₂ photofixation.

3.4. Carbonaceous materials

Metal-free semiconductor photocatalysts have triggered a renaissance of great interest since the advent of H-terminated

boron-doped (B-doped) diamond as a solid-state source of electrons in water for photo-driven N₂ fixation in 2013.¹⁶⁵ It was demonstrated that the UV excitation of B-doped diamond induced electron emissions and their ejection into liquids to produce solvated electrons which reacted quickly with protons to form neutral atomic hydrogen, H•, and finally facilitated the subsequent reaction with N₂ to yield NH₃. In this context, the photocatalytic activity decreased with time because the oxidation of the H-terminated surface to O-terminated resulted in a loss of electron affinity. The authors also revealed that photocatalytic behaviour could be observed using the natural diamond dispersed in water. Further study of the mechanism of action of aqueous solvated electrons was methodically reported in the following year.¹⁶⁶ Three possible reaction steps, including (1) electron transfer (N₂ + e⁻ → N₂⁻), (2) proton-coupled electron transfer (N₂ + e⁻ + H₂O → N₂H + OH⁻) and (3) hydrogen atom addition (N₂ + H• → N₂H), were proposed with the help of kinetic modelling. It was concluded that the reduction of N₂ to NH₃ involved hydrogen atom addition at the initial steps and protonation/electron transfer by solvated electrons at the later steps. In 2016, metal-diamond heterostructures (*i.e.* diamond thin films grown on Mo, Ni and Ti metal substrates) were reported. It was noted that some electrons excited from the metal substrates would be injected into the conduction band of the diamond film, followed by emission into water.¹⁶⁷

In the present literature, most research has focused a spotlight on carbonaceous nanomaterials. Benefiting from the rational significance of the oxygen vacancies in bismuth oxyhalides, as described in Section 3.3.,¹⁵¹ graphitic carbon nitride (g-C₃N₄) with nitrogen vacancies (NV-g-C₃N₄) has become a focal area in materials science since 2015.⁷³ Because they have the same shape and size as the nitrogen atoms in dinitrogen, nitrogen vacancies (NVs) are beneficial in the selective chemisorption and activation of N₂. This explains why the nitrogen fixation rate remained unchanged when N₂ was replaced by air as the N₂ source. In addition, NVs prominently improved the separation of charge carriers by trapping photogenerated electrons and promoting electron transfer to the adsorbed N₂.⁶² Following this astounding discovery, NV-g-C₃N₄ was extensively investigated based on manifold aspects, namely the modification of preparation routes for large-scale production and the enlargement of the specific surface area.^{168–171} Furthermore, modifications such as iron doping and ruthenium loading have been exhaustively explored in recent years.^{172,173} Similar to diamond, the H-termination of Ru-loaded g-C₃N₄ played an indispensable role in the activation of N₂.¹⁷⁰

Recently, g-C₃N₄ has been widely employed to construct heterostructure junctions with another component, including the hybridization of g-C₃N₄ with metal sulfides,^{154,155} metal oxides,^{174–176} and reduced graphene oxide (rGO).¹⁷⁷ As a proof of concept, multi-metal oxides with tunable band structures match favorably with other semiconductors when engineering intact heterojunction interfaces.¹⁷⁸ After assembly, the g-C₃N₄/MgAlFeO nanorod heterostructure was effective in N₂ photoreduction. In particular, a Z-scheme heterojunction was established, as depicted in Fig. 9a. In this instant, the photoexcited electrons

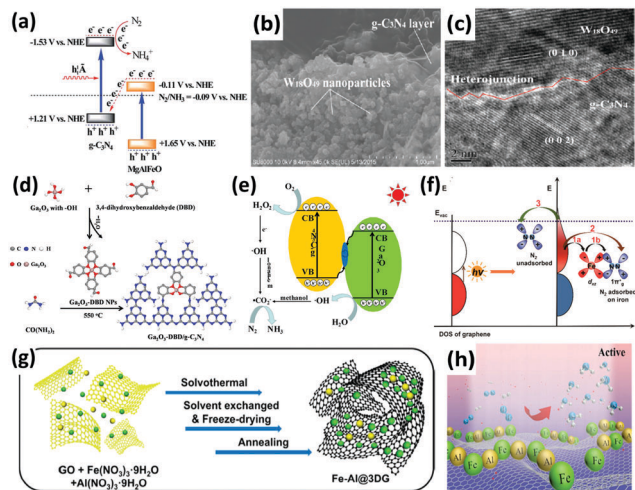


Fig. 9 (a) Tentative Z-scheme heterojunction interface of $g\text{-C}_3\text{N}_4/\text{MgAlFeO}$. Reproduced with permission.¹⁷⁴ Copyright 2017, Royal Society of Chemistry. (b) SEM and (c) HRTEM images of $\text{WO}_{18}\text{O}_{49}/g\text{-C}_3\text{N}_4$. Reproduced with permission.¹⁷⁵ Copyright 2017, Royal Society of Chemistry. (d) The formation process and (e) photocatalytic N_2 reduction mechanism of $\text{Ga}_2\text{O}_3\text{-DBD}/g\text{-C}_3\text{N}_4$. Reproduced with permission.¹⁷⁶ Copyright 2017, Elsevier. (f) Possible paths of photo-generated electrons from graphene for the activation of N_2 molecules. Reproduced with permission.¹⁸³ Copyright 2016, American Chemical Society. (g) Schematic of the synthesis procedure of the Fe-Al@3DG and (h) NH_3 synthesis over Fe-Al@3DG . Reproduced with permission.¹⁸⁴ Copyright 2017, Elsevier.

in the conduction band of MgAlFeO were transferred to the valence band of $g\text{-C}_3\text{N}_4$. Due to this phenomenon, the electrons in the conduction band of $g\text{-C}_3\text{N}_4$ did not recombine with the holes, instead participating in the N_2 reduction.¹⁷⁴ A similar Z-scheme heterojunction mechanism for N_2 fixation was reported in other studies: (1) $\text{W}_{18}\text{O}_{49}/g\text{-C}_3\text{N}_4$ catalyst (Fig. 9b and c) was active under near-infrared (NIR) irradiation¹⁷⁵ because of the coherent oscillations of the surface free electrons induced by the oxygen vacancies on $\text{W}_{18}\text{O}_{49}$. (2) 3,4-Dihydroxybenzaldehyde-functionalized $\text{Ga}_2\text{O}_3/\text{graphitic carbon nitride}$ ($\text{Ga}_2\text{O}_3\text{-DBD}/g\text{-C}_3\text{N}_4$), synthesized by incorporating $\text{Ga}_2\text{O}_3\text{-DBD}$ NPs into $g\text{-C}_3\text{N}_4$ networks (Fig. 9d),¹⁷⁶ was reported to be capable of converting N_2 to NH_3 with the aid of the strong reducing power of $\cdot\text{CO}_2^-$, which was formed by the oxidation of methanol by active oxygen species (Fig. 9e). In essence, this is similar to the N_2 reduction mechanism of $\beta\text{-Ga}_2\text{O}_3$, as discussed earlier in Fig. 5c.

As for two-dimensional (2D) graphene, a metal-free 2D/2D hybrid heterostructure of $g\text{-C}_3\text{N}_4/\text{rGO}$ was designed by coupling rGO and protonated $g\text{-C}_3\text{N}_4$, in which rGO served as a conducting substrate.¹⁷⁷ Protonated $g\text{-C}_3\text{N}_4$ exhibited 5 times the NH_3 production rate of pristine $g\text{-C}_3\text{N}_4$, and the activity was further ameliorated after assembly with rGO. It was deduced that the face-to-face contact area on the $g\text{-C}_3\text{N}_4/\text{rGO}$ heterointerface for enhanced charge transfer substantially decreased the electron-hole recombination rate of $g\text{-C}_3\text{N}_4$.¹⁷⁹ In essence, this finding is analogous to our previous studies on metal-free 2D/2D graphene/ $g\text{-C}_3\text{N}_4$ for CO_2 photoreduction, in which graphene acts as an excellent electron reservoir.^{180–182} There is another report on the loading of iron oxide on bulk three-dimensional (3D) cross-linked

graphene (Fe@3DG) for the reduction of N_2 to NH_3 under light irradiation.¹⁸³ Graphene played the role of generating highly energetic electrons. A significant enhancement of photocatalytic activity was observed by increasing the electron density of Fe due to its electron donation from the Fe d orbital to the anti-bonding orbital of N_2 (Fig. 9f).

Because the photoactivity of the Fe@3DG nanocomposite significantly decreased after 5 hours of reaction, in 2017, the same research group modified the existing Fe@3DG nanocomposite by incorporating Al_2O_3 to form Fe-Al@3DG photocatalysts (Fig. 9g).¹⁸⁴ Al_2O_3 functioned as an excellent dispersing agent and barrier to prevent the aggregation of Fe_2O_3 nanoparticles on the 3D graphene (Fig. 9h). Fascinatingly, the NH_3 production yield of 20Fe-2Al@3DG (20 wt% Fe and 2 wt% Al) remained steady even after 60 hours of light-driven reaction, which was more than two times that of the parent 20Fe@3DG (20 wt% Fe), demonstrating the salient role of Al_2O_3 as a structural promoter. In general, the employment of 2D/2D heterojunction interfaces and 3D nanoarchitecture design for photocatalysis based on the motivation of effective charge carrier transfer and separation is still in the infant stage. Furthermore, most existing literature studies focus on 0D/2D hybrid nanostructures. Therefore, extensive studies in this related field are imperative to achieve excellent prospects in addressing the limitations of this process for scientific merit and to enhance fundamental research knowledge toward realizing industrialization in the future.

3.5 Other potential materials

Gallium phosphide is a typical semiconductor that has been researched in the photocatalytic field for a long time.^{185,186} In 1978, Dickson *et al.* employed a photoelectrochemical cell to perform N_2 fixation.¹⁸⁷ The system consisted of a p-GaP cathode and an aluminum metal anode immersed in a non-aqueous electrolyte of titanium tetraisopropoxide and AlCl_3 dissolved in glyme. In this system, the p-GaP electrode absorbed light and provided the activation energy for the photoenhanced reduction of N_2 . In 1980, Miyama *et al.* reported the performance of GaP and GaP/Pt for the reduction of N_2 . In fact, a few researchers have already implemented the reduction of N_2 on GaP nanoparticles without light.¹⁰⁴

Zeolites have also been applied in the photochemical synthesis of NH_3 from N_2 . Khan *et al.* reported the production of ammonia with titanium-exchanged zeolites under visible light.¹⁸⁸ Two years later, they tested the exchange of different types of zeolites with titanium ions. It is noteworthy that the Ti^{3+} ions contributed to the reduction of N_2 for the oxidation of Ti^{3+} to Ti^{4+} .¹⁸⁹ Furthermore, the NH_3 production was reported to increase with increasing re-exchange time of the zeolites by Ti^{3+} .

As mentioned above,^{127,128} localized surface plasmon resonance (LSPR) of metal particles has also been utilized to drive the photoabsorption of other catalysts. In 2014, Zeng *et al.* applied catalytically active metal (Os) directly to LSPR Au particles (Os-Au nanocomposites) for the NH_3 synthesis reaction.¹⁹⁰ It was found that the Au nanoparticles with superior LSPR absorbance and photoabsorption did not show any catalytic activity, while Os nanoparticles with high catalytic activity

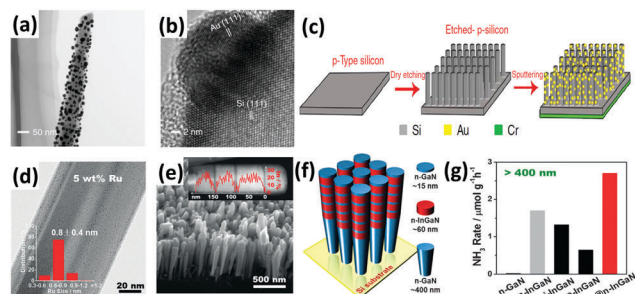


Fig. 10 (a) TEM and (b) HRTEM images of a GNPs-coated p-type silicon nanowire. (c) Schematic of the fabrication of the GNP/bSi/Cr photoelectric cell. Reproduced with permission.¹⁹¹ Copyright 2016, Nature Publishing Group. (d) TEM image of the 5 wt% Ru-modified GaN NWs (inset plot shows the diameter distributions of the Ru sub-nanoclusters). (e) SEM image of the developed InGaN/GaN nanowires on the Si (111) substrate. (f) Schematic of the InGaN/GaN nanowire structure. (g) Rate of NH₃ generation over various III-nitride semiconductors under visible light irradiation ($\lambda > 400$ nm). Reproduced with permission.¹⁹² Copyright 2017, Wiley-VCH.

could not absorb photoenergy. By allying the concept of LSPR Au particles with the active metal (Os), the Os–Au nanohybrids outperformed the individual components, thus improving the solar light utilization for the chemical synthesis of NH₃. In 2016, a solar-driven photoelectrochemical cell based on plasmon-enhanced black silicon (bSi) was documented by MacFarlane's group.¹⁹¹ The plasmon-enhanced bSi was decorated with Au nanoparticles (GNPs) and a layer of Cr (Fig. 10a–c). In the GNP/bSi/Cr photoelectrochemical cell, bSi, GNPs and Cr performed as photoabsorber, reduction catalysis sites and hole-sink layer, respectively. The bSi ameliorated the scattering and absorption of light and provided a sufficient surface area for the decoration of a large amount of GNPs. From the charge transfer mechanism, the GNPs accumulated photogenerated electrons, whereas Cr acted as a sacrificial anode to gather holes. This research resulted in hundreds of times improvement in the NH₃ production rate compared with plasmon-induced photoelectrodes (Au NPs/Nb–SrTiO₃/Ru and Au NPs/Nb–SrTiO₃/Zr/ZrO_x), as mentioned in Section 3.1.3.^{127,128}

A similar one-dimensional (1D) structure of gallium nitride nanowires (GaN NWs) grown on a silicon (Si) substrate was very recently designed by Li and co-workers.¹⁹² The Ge-doped n-type GaN NWs exhibited improved N₂ photofixation activity under UV irradiation with the aid of ultras-small Ru clusters of *ca.* 0.8 nm (Fig. 10d). After the incorporation of Ru, the photo-excited electrons were facily transferred from the III-nitride semiconductors to Ru as a result of an effective interfacial metal/semiconductor Schottky junction with a barrier height of 0.94 eV, thus demonstrating the role of Ru as an electron reservoir to facilitate the cleavage of N≡N triple bonds. Furthermore, the band gap was shifted to the visible light region (2.34 eV) by introducing In (*ca.* 25% composition) into GaN NWs, forming 5 segments of n-type InGaN NWs on the GaN NW template (Fig. 10e and f). Assisted by Ru sub-nanoclusters, the photoactivity of n-type InGaN/n-GaN toward NH₃ synthesis was the highest compared to other reference samples under visible light irradiation ($\lambda > 400$ nm) (Fig. 10g). For ease of comparison of the

selected literature studies, Tables 2 and 3 summarize most of the photocatalysts, including metal oxide-based, metal sulfide-based, bismuth oxyhalides (BiOX), and metal-free carbonaceous nanomaterials.

4. Concluding remarks

The photoreduction of N₂ to NH₃ is regarded as a scientifically challenging yet environmentally friendly technology for the sustainable growth of the human population. NH₃ has elicited much research fascination and broad interdisciplinary attention as a hydrogen carrier in addition to its wide use as an industrial raw material and fertilizer.^{193,194} In this review article, we have thoroughly presented and classified a diverse selection of photocatalysts for N₂ fixation. The selected literature reports are summarized in Tables 2 and 3. Overall, we genuinely envision that this review will establish benchmarks and mitigate the present obstacles in N₂ photoreduction as well as broaden new inroads at the forefront of this research hotspot. In order to optimize the practical schemes, several concluding remarks, prospects and suggestions are elucidated.

(I) Pre-treatment

In the study of iron-doped TiO₂, it is apparent that the N₂ reduction photocatalytic activity is highly dependent on the pre-treatment method of the as-developed catalysts. The different preparation techniques are presented in Table 4. On the one hand, the synthetic routes markedly influence the photocatalytic activity based on a plethora of aspects, including chemical compounds, defects, crystal morphologies and particle sizes. Additionally, heat treatment plays a central role in the physico-chemical properties of the nanomaterials. Notably, annealing at a high temperature introduces defect states, which enhance the photoreduction ability.⁹¹ In another aspect, prolonged heat treatment adversely affects the phase transformation and the amount of surface •OH groups, which is detrimental to the activity of photocatalysts.⁶⁷ As described earlier, the treatment of catalysts in H₂ atmosphere will contribute to an increase of H_{ads} on the surface or even form an H-terminated surface, thus facilitating the hydrogenation of nitrogen. However, the amount of surficial H will decrease with time, leading to suppressed photoactivity.

(II) Reaction mixture

In addition to the gas-phase reaction, aqueous-phase photo-reaction has also been widely employed *via* the suspension of photocatalysts in liquid. An aqueous slurry with an appropriate concentration of photocatalyst enhances the photoreaction by accelerating the dispersion of the photocatalyst for improved mass transfer. However, high concentrations lead to poor penetration of photons.⁹⁶ It has also been reported that in the presence of photocatalysts, the •OH radicals in water oxidize ammonia to nitrate.¹²⁵ As such, ammonia and nitrate are detected in the final products of photoreaction.¹³³

Table 2 Summary of metal oxide-based photocatalysts for the reduction of N₂ to NH₃(l)

	Year	Catalyst	T (K)	Light source	Nitrogen source	Organic scavenger	NH ₃ average r_{NH_3}	Author	Ref.
TiO ₂ -Based Materials	1997	0.2 wt% Fe-doped TiO ₂	313	390–420 nm	N ₂	None	10 $\mu\text{mol g}^{-1} \text{h}^{-1}$	Schrauzer	67
	1988	TiO ₂	500	UV	N ₂	None	0.83 $\mu\text{mol g}^{-1} \text{h}^{-1}$	Bourgeois	91
	1991	0.5 wt% Fe-doped TiO ₂	353	UV	N ₂	None	6 $\mu\text{mol g}^{-1} \text{h}^{-1}$	Soria	98
	2014	Fe-doped TiO ₂ (Fe/Ti = 10 ⁻⁴)	298	$\lambda = 254 \text{ nm}$	Air	Ethanol	1 $\text{g}_{\text{cat}} \text{L}^{-1}$; 400 $\mu\text{M h}^{-1}$	Zhao	99
	2017	JRC-TiO-6 (rutile)	313	$\lambda > 254 \text{ nm}$	N ₂	2-PrOH ^e	1 $\text{g}_{\text{cat}} \text{L}^{-1}$; 2.5 $\mu\text{M h}^{-1}$	Hirakawa	92
	1977	0.4 wt% Co-doped TiO ₂	313	UV	N ₂	None	6.3 $\mu\text{mol g}^{-1} \text{h}^{-1}$	Schrauzer	67
	1977	0.4 wt% Mo-doped TiO ₂	313	UV	N ₂	None	6.7 $\mu\text{mol g}^{-1} \text{h}^{-1}$	Schrauzer	67
	1977	0.4 wt% Cr-doped TiO ₂	313	UV	N ₂	None	0.37 $\mu\text{mol g}^{-1} \text{h}^{-1}$	Schrauzer	67
	1988	0.5 wt% Cr-doped TiO ₂	353	UV	N ₂	None	2.6 $\mu\text{mol g}^{-1} \text{h}^{-1}$	Palmisano	100
	1990	2 wt% Mg-doped TiO ₂	—	UV	N ₂	None	0.67 $\text{g}_{\text{cat}} \text{L}^{-1}$; 6.9 $\mu\text{M h}^{-1}$	Ileperuma	102
	1993	10 wt% V-doped TiO ₂	—	UV	N ₂	None	0.8 $\text{g}_{\text{cat}} \text{L}^{-1}$; 4.9 $\mu\text{M h}^{-1}$	Ileperuma	103
	1993	10 wt% Ce-doped TiO ₂	—	UV	N ₂	None	0.8 $\text{g}_{\text{cat}} \text{L}^{-1}$; 3.4 $\mu\text{M h}^{-1}$	Ileperuma	103
	1996	0.24 wt% Ru-loaded TiO ₂	—	UV-vis	N ₂	Ethanol	22.7 $\mu\text{mol g}^{-1} \text{h}^{-1}$	Ranjit	106
	2001	TiO ₂ /P3MeT	293	UV	N ₂	None	—	Hoshino	109
	2008	5% RuCl ₃ -modified TiO ₂	rt ^c	UV-vis	N ₂	Humic acid	4 $\mu\text{M h}^{-1} \text{cm}^{-2a}$	Linnik	109
Other binary oxides	1987	Partially reduced Fe ₂ O ₃	303	UV-vis	N ₂	None	10 $\mu\text{mol g}^{-1} \text{h}^{-1}$	Khader	111
	2010	Pt-loaded ZnO	—	UV	N ₂	Na-EDTA ^f	860 $\mu\text{mol g}^{-1} \text{h}^{-1}$	Janet	118
	2015	Mesoporous β -Ga ₂ O ₃ nanorods	298	$\lambda = 254 \text{ nm}$	N ₂ /O ₂	TBA ^g	$\phi = 36.1\%d$	Zhao	115
	2017	Fe ₂ O ₃	298	UV-vis	N ₂	Ethanol	0.5 $\text{g}_{\text{cat}} \text{L}^{-1}$; 1362.5 $\mu\text{M h}^{-1}$	Lashgari	113
	2017	BiO quantum dots	298	UV-vis	N ₂	None	0.25 $\text{g}_{\text{cat}} \text{L}^{-1}$; 50.5 $\mu\text{M h}^{-1}$	Sun	116
Ternary metal oxides	1983	BaTiO ₃	313	UV	N ₂	None	0.87 $\mu\text{mol g}^{-1} \text{h}^{-1}$	Li	125
	1983	RuO ₂ -NiO-BaTiO ₃	313	UV	N ₂	None	2.6 $\mu\text{mol g}^{-1} \text{h}^{-1}$	Li	125
	2001	Iron titanate films (Fe/Ti = 1 : 1)	—	$\lambda \geq 320 \text{ nm}$	N ₂	Ethanol	0.57 $\mu\text{M h}^{-1} \text{cm}^{-2a}$	Rusina	121
	2014	Au NPs/Nb-SrTiO ₃ /Ru	rt ^c	550–800 nm	N ₂	Ethanol	1.1 $\text{nmol h}^{-1} \text{cm}^{-2}$	Oshikiri	127
	2016	Au NPs/Nb-SrTiO ₃ /Zr/ZrO _x	rt ^c	550–800 nm	N ₂	Ethanol	6.5 $\text{nmol h}^{-1} \text{cm}^{-2}$	Oshikiri	128
	2016	H-Bi ₂ MoO ₆	rt ^c	Sunlight	Air	None	1300 $\mu\text{mol g}^{-1} \text{h}^{-1}$	Hao	131
Hydrous oxides	1987	Fe ₂ O ₃ (H ₂ O) _n	—	Vis	N ₂	None	6 $\mu\text{M h}^{-1b}$	Tennakone	132
	1988	Hydrous oxides of Fe(III) and Ti(IV) (Ti : Fe = 8%)	—	Vis	N ₂	None	22 $\mu\text{M h}^{-1b}$	Tennakone	138
	1989	Cu ₂ O·xH ₂ O·CuCl	—	UV	N ₂	None	70 $\mu\text{M h}^{-1b}$	Tennakone	134
	1991	Fe(O)OH	—	UV	N ₂	None	9.25 $\mu\text{M h}^{-1b}$	Tennakone	133
	1991	Bentonite-hydrous ferric oxide	—	UV	N ₂	None	2 $\text{g}_{\text{cat}} \text{L}^{-1}$; 1.33 $\mu\text{M h}^{-1}$	Ilepruma	137
	1992	V(III)-substituted hydrous ferric oxide	299	UV	N ₂	None	8.33 $\mu\text{M h}^{-1b}$	Tennakone	139
	1993	Sm ₂ O ₃ ·xH ₂ O/V ₂ O ₅ ·xH ₂ O	299	UV	N ₂	None	100 $\mu\text{M h}^{-1b}$	Tennakone	135
	2016	Carbon-tungstic acid hybrids	—	UV-vis	N ₂	None	205 $\mu\text{mol g}^{-1} \text{h}^{-1b}$	Li	136

^a The unit $\text{mM h}^{-1} \text{cm}^{-2}$ is not standardized because the volume of the solution was not given in the literature. ^b The catalyst cannot be weighed because it denatures upon drying. ^c rt denotes room temperature. ^d ϕ = apparent quantum yield. ^e 2-PrOH denotes 2-propanol. ^f EDTA denotes ethylenediaminetetraacetic acid. ^g TBA denotes *tert*-butanol.

The presence of organic scavengers such as ethanol and methanol can obviously increase the NH₃ yield by providing sacrificial electron donors to the holes in the semiconductor.¹²³ As for the side reaction of the sacrificial agent, Rusina *et al.* inferred that ethanol facilitates the formation of nitrite and nitrate,¹²¹ while Zhao and Lashgari claimed that ethanol serves as a superior •OH scavenger which protects the NH₃ yield from further oxidation to its higher oxidation states of nitrite or nitrate (Fig. 11).^{99,113} Usually, holes react with hydroxide ions to form hydroxyl radicals ($\text{OH}^- + h_{\text{VB}}^+ \rightarrow \bullet\text{OH}$), which can further oxidize NH₃. In this regard, when ethanol is present, it can be oxidized to CH₃CHO and C₂H₅OC₂H₅.⁹⁹ Along with the consumption of photo-generated holes in an oxidation process, the N₂ reduction rates can be markedly increased due to the availability of abundant photo-generated electrons for the reduction reactions. Although ethanol is generally utilized as a typical organic scavenger, it is crucial to comprehensively

study different alcohols in order to determine suitable sacrificial agents for specific light-driven catalytic systems.

(III) Modification of semiconductors

Transition metals are widely used as dopants, co-catalysts and plasmonic nanostructures with the aim of enhancing photocatalytic efficiency. Among these, earth-abundant iron is the most dominant as an efficient metal dopant. In contrast, it has been reported that noble metals as dopants in TiO₂ demonstrate inhibiting effects for N₂ photoreduction.⁶⁷ Moreover, this inhibiting effect has been observed on Pt-loaded ZnO compared with pure ZnO.¹⁰⁴ However, the incorporation of Ru as a co-catalyst on semiconductors has exhibited an evident positive influence on N₂ fixation activity.¹⁰⁶ Recently, plasmonic metals were reported to enhance photoabsorption *via* LSPR. To date, Au has been selected to couple with myriad catalysts, such as SrTiO₃,^{127,128} Os and black silicon,^{190,191} because its

Table 3 Summary of other types of photocatalysts for the reduction of N₂ to NH₃(l)

	Year	Catalyst	<i>T</i> (K)	Light source	Nitrogen source	Organic scavenger	NH ₃ average r_{NH_3}	Author	Ref.
BiOX	2015	BiOCl	298	UV-vis	N ₂	Methanol	0.67 g _{cat} L ⁻¹ ; 46.2 μM h ⁻¹	Li	88
	2015	BiOBr	298	Vis	N ₂	None	0.5 g _{cat} L ⁻¹ ; 1042 μM h ⁻¹	Li	151
	2016	Bi ₅ O ₇ I	293	UV-vis	N ₂	Methanol	0.5 g _{cat} L ⁻¹ ; 111.5 μM h ⁻¹	Bai	89
	2017	Bi ₅ O ₇ Br nanotubes	rt ^b	λ > 400 nm	N ₂	None	1380 μmol g ⁻¹ h ⁻¹	Wang	164
Metal sulfides	1980	CdS/Pt	311	UV	N ₂	None	3.26 μmol g ⁻¹ h ⁻¹	Miyama	104
	1988	CdS/Pt/RuO ₂	303	λ ≥ 505 nm	N ₂	None	4 g _{cat} L ⁻¹ ; 620 μM h ⁻¹	Khan	144
	1990	Pt/CdS-Ag ₂ S/RuO ₂	303	UV-vis	N ₂	None	2 g _{cat} L ⁻¹ ; 1260 μM h ⁻¹	Khan	145
	2015	[Mo ₂ Fe ₆ S ₈ (SPh) ₃] ³⁺ -[Sn ₂ S ₆] ⁴⁻	rt ^b	UV-vis	N ₂	—	10.1 μM h ^{-1 a}	Banerjee	148
	2016	Mo ₂ Fe ₆ S ₈ (SPh) ₃ -Fe ₄ S ₄ [Sn ₂ S ₆] ⁴⁻	rt ^b	UV-vis	N ₂	—	18.82 μM h ^{-1 a}	Liu	149
	2016	CdS/MoFe protein	—	λ = 405 nm	—	None	315 μmol g _{protein} ⁻¹ min ⁻¹	Brown	147
	2016	Zn _{0.1} Sn _{0.1} Cd _{0.8} S	303	400–800 nm	N ₂	Ethanol	0.4 g _{cat} L ⁻¹ ; 105.2 μM h ⁻¹	Hu	152
	2016	Mo _{0.1} Ni _{0.1} Cd _{0.8} S	303	400–800 nm	N ₂	Ethanol	0.4 g _{cat} L ⁻¹ ; 71.2 μM h ⁻¹	Cao	153
	2016	g-C ₃ N ₄ /ZnSnCdS	303	400–800 nm	N ₂	Ethanol	0.4 g _{cat} L ⁻¹ ; 167.6 μM h ⁻¹	Hu	154
	2016	g-C ₃ N ₄ /ZnMoCdS	298	400–800 nm	Air	Ethanol	0.4 g _{cat} L ⁻¹ ; 77.6 μM h ⁻¹	Zhang	155
	2016	Ni ₂ P/Cd _{0.5} Zn _{0.5} S	293	λ ≥ 400 nm	N ₂	None	0.4 g _{cat} L ⁻¹ ; 101.5 μM h ⁻¹	Ye	146
	2016	MoS ₂	298	λ ≥ 420 nm	N ₂	None	325 μmol g ⁻¹ h ⁻¹	Sun	159
Carbonaceous materials	2013	Boron-doped diamond	—	UV	N ₂	None	—	Zhu	165
	2015	g-C ₃ N ₄	—	λ ≥ 420 nm	Air	Methanol	1 g _{cat} L ⁻¹ ; 160 μM h ⁻¹	Dong	62
	2016	g-C ₃ N ₄ /rGO	303	400–800 nm	Air	Na-EDTA ^c	0.4 g _{cat} L ⁻¹ ; 206 μM h ⁻¹	Hu	177
	2016	Fe-loaded 3D graphene	473	UV	N ₂ /H ₂	None	24 μmol g ⁻¹ h ⁻¹	Lu	183
	2017	Fe-Al-loaded 3D graphene	473	UV	N ₂ /H ₂	None	25.3 μmol g ⁻¹ h ⁻¹	Yang	184
	2017	Fe-doped g-C ₃ N ₄	303	400–800 nm	N ₂	Ethanol	0.4 g _{cat} L ⁻¹ ; 120 μM h ⁻¹	Hu	172
	2017	g-C ₃ N ₄ /MgAlFeO	303	400–800 nm	N ₂	Ethanol	0.4 g _{cat} L ⁻¹ ; 166.8 μM h ⁻¹	Wang	174
	2017	W ₁₈ O ₄₉ /g-C ₃ N ₄	—	UV-vis-NIR ^d	N ₂	Ethanol	0.4 g _{cat} L ⁻¹ ; 57.8 μM h ⁻¹	Liang	175
	2017	Ga ₂ O ₃ -DBD/g-C ₃ N ₄	—	UV-vis	N ₂	Ethanol	0.4 g _{cat} L ⁻¹ ; 112.5 μM h ⁻¹	Cao	176
Other system	1980	GaP/Pt	311	UV	N ₂	None	5 μmol g ⁻¹ h ⁻¹	Miyama	104
	1981	Ti ³⁺ -exchanged zeolites	—	Vis	N ₂	None	20.6 μmol g ⁻¹ h ⁻¹	Khan	188
	1983	Ti ³⁺ -exchanged zeolites	~305	Vis	N ₂	None	32.9 μmol g ⁻¹ h ⁻¹	Khan	189
	2015	Cs ₂ O-promoted Os-Au	333	λ ≥ 450 nm	N ₂ /H ₂	None	2685 μmol g ⁻¹ h ⁻¹	Zeng	190
	2016	GNP/bSi/Cr	—	UV-vis	N ₂	None	0.78 μmol h ⁻¹ cm ⁻²	Ali	191
	2017	5% Ru@n-GaN NWs	283	290–380 nm	N ₂	None	120 μmol g ⁻¹ h ⁻¹	Li	192

^a The catalyst cannot be weighed because it denatures upon drying. ^b rt denotes room temperature. ^c EDTA denotes ethylenediaminetetraacetic acid. ^d Using optical filters, light of λ > 800 nm and λ < 800 nm was removed for the 300 W Xenon lamp and 200 W infrared light source, respectively, to simulate full-spectrum light.

Table 4 Typical pre-treatment methods for iron-doped TiO₂^{67,98,99,121}

Year	Author	Preparation procedures
1977	Schrauzer	Calcine iron sulfate impregnated with anatase TiO ₂ at 1273 K for 1 h in air
1991	Soria	Coprecipitate solution of TiCl ₃ and iron ions in an NH ₃ solution and anneal the resulting solid at 823 K for 24 h
2001	Rusina	React iron chloride with tetraisopropyl titanate in a sol-gel method and calcine the resulting solid at 923 K for 20 min
2014	Zhao	Incorporate Fe ³⁺ into hydrogen titanate phase nanotubes <i>via</i> a hydrothermal method followed by performing calcination at 773 K for 3 h

light-harvesting effects can efficiently utilize the visible light region of the solar spectrum.

Additionally, the flourishing investigation of oxygen vacancies induced in BiOX has inspired many researchers due to their unique characteristics for the efficient separation of charge carriers. As illustrated in Fig. 12,¹⁵¹ OV s suppress the recombination of electrons and holes by directly trapping electrons from the conduction band and then transferring them to the anti-bonding orbitals of adsorbed N₂. Since the first seminal report on oxygen vacancies in BiOBr for N₂ fixation in 2015, a number of studies on nitrogen, sulfur and oxygen vacancies have been reported to date.^{62,152,154} As a proof of concept, a hybrid structure is always desirable for modulating band structures for ameliorated solar energy conversion.^{195–203} Importantly, the

heterostructure will spatially accumulate the separation and transfer of photogenerated charge carriers upon their interactions at the contacted interface.

(IV) Suggestions, outlook and future prospects

As shown in Table 2, the assessments of photocatalytic activities for N₂ reduction are not unified. The standard NH₃ production rate can be expressed in units of μmol h⁻¹ g⁻¹ for the gas-phase reaction, μM h⁻¹ for the reaction in solution and μmol h⁻¹ cm⁻² for photoelectrochemical cells. Therefore, apparent quantum yield (AQY) should be generalized as a scientific tool to account for dissimilar experimental conditions, such as light source, catalyst loading, reaction duration and illumination area.

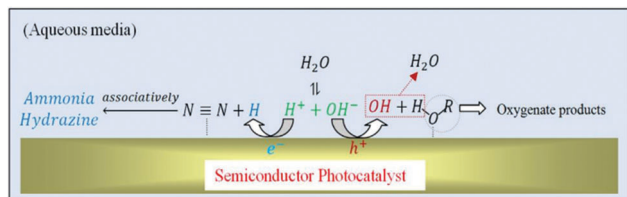


Fig. 11 Schematic of the reaction mechanism of N_2 fixation at the semiconductor/solution interface in the presence of alcohol as a sacrificial agent. Reproduced with permission.¹¹³ Copyright 2017, Elsevier.

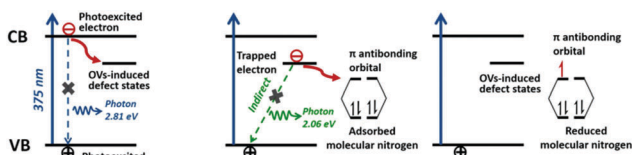


Fig. 12 Schematic of the enhancement of OV-induced photocatalysts for interfacial electron transfer processes. Reproduced with permission.¹⁵¹ Copyright 2015, American Chemical Society.

Most previous studies have focused on metal oxide-based nanomaterials, especially in the case of TiO_2 . However, TiO_2 is greatly restricted by its UV excitation, which constitutes less than 5% of the solar light spectrum. Additionally, Cd-containing dichalcogenides are mostly in the form of sulfides, while the stability of CdS urgently requires improvement by forming multi-metal systems. Furthermore, air and visible light are gradually being adopted as nitrogen and light sources instead of pure nitrogen and UV irradiation. In order to use air as the N_2 source, the selectivity of the desired products should be taken into consideration to avoid the side product of H_2 evolution and the decomposition of NH_3 . In contrast, for the aqueous-phase reaction, more attention should be paid to the nitrite and nitrate contents in the products. In addition, research on metal-free systems has been primarily dominated by g- C_3N_4 to date. Although in-depth studies on band structures and charge carrier dynamics are necessary, the exploration of new potential photocatalysts is gaining in momentum to surmount the bottlenecks of the fundamental research and applications of N_2 fixation. It is our aim to extend the utilization and optical absorption of solar light up to the NIR in addition to UV and visible light to cater to the entire spectrum of solar light.

In other aspect, a robust device for assembling different components is overwhelmingly necessary to develop a multi-functional platform for artificial photosynthesis – N_2 fixation. The engineering of an intact “machine” should comprise a N_2 reduction catalyst, an oxidation catalyst, a light-harvesting absorber and an electron-transporting bridge to attain high photocatalytic efficiency of N_2 fixation. Therefore, the synergetic interactions of various moieties within an individual matrix must be taken into consideration. Good examples of such versatile “machines” include porous metal-organic frameworks (MOFs) and covalent organic frameworks (COFs), to which further exploration should be devoted in the future. Apart from photon-driven catalysis, with the aid of external bias, a photoelectrocatalytic

system is another smart avenue to separate the redox reactions (*i.e.* N_2 reduction and H_2O oxidation) at the photocathode and photoanode, respectively. Unequivocally, there is an extreme paucity of literature reports on photoelectrochemical N_2 fixation at the moment. Thus, a combined light-driven and electro-driven reaction would undeniably greatly facilitate N_2 fixation activity. To this end, dissimilar photocatalysts at the cathode and anode sides could be designed. Essentially, with the present knowledge on the electrochemical reduction of N_2 based on a wealth of research activities to date, this provides a scientific guiding star for photoelectrochemical N_2 reduction systems.

For heterogeneous photocatalytic systems, insights into their reaction pathways are essential, despite the complexity of the N_2 fixation reaction. It is prominent that tuning the size of photocatalysts can remarkably alter the ratio of exposed atoms and active sites on the corners, edges and surfaces with different coordination numbers. As a result, this influences the adsorption ability of the reactant N_2 molecules as well as the intermediates during the photoreduction process, giving rise to dissimilar performance and activity of the shape- and size-controlled photocatalysts. To comprehend the atomic insights in reactivity, advanced *in situ* or *operando* characterization techniques are indispensable. For example, *in situ* FTIR analysis is beneficial to examine the adsorbed nitrogen species on the surface of photocatalysts. Meanwhile, environmental/*in situ* TEM and X-ray absorption spectroscopy can provide information on the structure evolution and the modification of the surface coordination number during the photocatalytic reaction process. Equally importantly, time-resolved spectroscopy, femtosecond transient absorption spectroscopy and terahertz time-domain spectroscopy would be helpful to study the excited-state dynamics in a typical photoinduced electron-transfer pathway. Additionally, computer-aided catalyst design *via* DFT calculations for N_2 fixation would be a robust tool for simulating band structures and reaction mechanisms to achieve excellent sunlight absorption and unprecedented catalysis performance. This could in turn provide auspicious references for the rational experimental design of photocatalysts. Therefore, the innovative engineering of photocatalysts from experimental and theoretical aspects is crucial to systematically tune the band gap for effective absorption of solar photon flux as well as high photoactivity for solar energy conversion.

In summary, it is evident that the product yield of N_2 photoreduction has gradually increased from a magnitude of $\mu\text{mol g}^{-1}$ to mmol g^{-1} . Without a doubt, the goal of achieving a magnitude of mol g^{-1} for the product yield will no longer be a dream; instead, this dream will be transformed into reality and practicality. Judging from the amount of existing literature on this research platform at this juncture, N_2 photoreduction has ignited interest and attention in the research community in recent years. However, it should be emphasized that the quantity of samples obtained from each batch is still at the laboratory scale. To divert from the laboratory-scale level to industrial applications, amplifying the yield of catalysts while retaining their intrinsic original structures is a global challenge. More thought should be given to translating these studies from

academic research to practicality. Despite the aforementioned impediments to the photoactivation of N_2 , the future direction of this area is indisputably promising and prospective with the synergetic cooperation of international researchers from diversified disciplines, such as computational scientists, chemists, materials scientists and physicists. Overall, we strongly believe that solar energy conversion for N_2 fixation will be enriched to begin a revolution of renewable energy for practical benefits and future commercialization.

Regarding the long-term prospects, there is an infinite scope of daunting challenges and opportunities for global researchers to expand the fundamental science at the forefront of this research hotspot. We are certain that this review article will provide an excellent basis for the next research era not only in photocatalytic N_2 fixation specifically, but also in the interdisciplinary fields of chemistry, materials science, energy conversion and energy storage. On the whole, with ceaseless determination and efforts from a diverse range of scientific communities and accomplishments in years to come, the research that has been comprehensively discussed in this review article will unquestionably be surpassed.

Conflicts of interest

There are no conflicts to declare.

Acknowledgements

N. Li is grateful for financial support from China Scholarship Council (CSC) with No. 201606955033, National Natural Science Foundation of China (NSFC) with No. 51461135004, Natural Science Foundation of Hubei Province with No. 2015CFB227, Fundamental Research Funds for the Central Universities, and the research board of the State Key Laboratory of Silicate Materials for Architectures. W.-J. Ong is also thankful for support from the Institute of Materials Research and Engineering (IMRE), Agency for Science, Technology and Research (A*STAR) in Singapore.

References

- V. Rosca, M. Duca, M. T. de Groot and M. T. M. Koper, *Chem. Rev.*, 2009, **109**, 2209–2244.
- D. E. Canfield, A. N. Glazer and P. G. Falkowski, *Science*, 2010, **330**, 192.
- B. K. Burgess and D. J. Lowe, *Chem. Rev.*, 1996, **96**, 2983–3012.
- H.-P. Jia and E. A. Quadrelli, *Chem. Soc. Rev.*, 2014, **43**, 547–564.
- A. Shilov, *Russ. Chem. Bull.*, 2003, **52**, 2555–2562.
- V. Smil, *Nature*, 1999, **400**, 415.
- B. M. Hoffman, D. Lukoyanov, Z.-Y. Yang, D. R. Dean and L. C. Seefeldt, *Chem. Rev.*, 2014, **114**, 4041–4062.
- C. N. Satterfield, *Heterogeneous Catalysis in Practice*, McGraw-Hill Companies, 1980.
- R. Schlögl, *Angew. Chem., Int. Ed.*, 2003, **42**, 2004–2008.
- H. Liu, *Chin. J. Catal.*, 2014, **35**, 1619–1640.
- M. Temkin and V. Pyzhev, *Acta Physiochim. U. R. S. S.*, 1940, **12**, 217–222.
- C. Liang, Z. Wei, Q. Xin and C. Li, *Appl. Catal., A*, 2001, **208**, 193–201.
- A. Vojvodic, A. J. Medford, F. Studt, F. Abild-Pedersen, T. S. Khan, T. Bligaard and J. K. Nørskov, *Chem. Phys. Lett.*, 2014, **598**, 108–112.
- Y. Inoue, M. Kitano, K. Kishida, H. Abe, Y. Niwa, M. Sasase, Y. Fujita, H. Ishikawa, T. Yokoyama and M. Hara, *ACS Catal.*, 2016, **6**, 7577–7584.
- A. D. Allen and C. V. Senoff, *Chem. Commun.*, 1965, 621–622.
- D. V. Yandulov and R. R. Schrock, *Science*, 2003, **301**, 76–78.
- G. Schwarz, R. R. Mendel and M. W. Ribbe, *Nature*, 2009, **460**, 839–847.
- K. Arashiba, Y. Miyake and Y. Nishibayashi, *Nat. Chem.*, 2011, **3**, 120–125.
- J. S. Anderson, J. Rittle and J. C. Peters, *Nature*, 2013, **501**, 84–87.
- S. E. Creutz and J. C. Peters, *J. Am. Chem. Soc.*, 2014, **136**, 1105–1115.
- J. Rittle and J. C. Peters, *J. Am. Chem. Soc.*, 2016, **138**, 4243–4248.
- T. Shima, S. Hu, G. Luo, X. Kang, Y. Luo and Z. Hou, *Science*, 2013, **340**, 1549–1552.
- B. M. Hoffman, D. R. Dean and L. C. Seefeldt, *Acc. Chem. Res.*, 2009, **42**, 609–619.
- R. Björnsson, F. Neese, R. R. Schrock, O. Einsle and S. DeBeer, *J. Biol. Inorg. Chem.*, 2015, **20**, 447–460.
- K. C. MacLeod and P. L. Holland, *Nat. Chem.*, 2013, **5**, 559–565.
- V. Kyriakou, I. Garagounis, E. Vasileiou, A. Vourros and M. Stoukides, *Catal. Today*, 2017, **286**, 2–13.
- G. Marnellos and M. Stoukides, *Science*, 1998, **282**, 98–100.
- Z. Li, R. Liu, Y. Xie, S. Feng and J. Wang, *Solid State Ionics*, 2005, **176**, 1063–1066.
- E. Vasileiou, V. Kyriakou, I. Garagounis, A. Vourros, A. Manerbino, W. G. Coors and M. Stoukides, *Top. Catal.*, 2015, **58**, 1193–1201.
- E. Vasileiou, V. Kyriakou, I. Garagounis, A. Vourros and M. Stoukides, *Solid State Ionics*, 2015, **275**, 110–116.
- Y. Kobayashi, N. Shimoda, Y. Kimura and S. Satokawa, *ECS Trans.*, 2017, **75**, 43–52.
- V. Kordali, G. Kyriakou and C. Lambrou, *Chem. Commun.*, 2000, 1673–1674.
- G. Xu, R. Liu and J. Wang, *Sci. China, Ser. B: Chem.*, 2009, **52**, 1171–1175.
- R. Lan and S. Tao, *RSC Adv.*, 2013, **3**, 18016–18021.
- T. Murakami, T. Nishikiori, T. Nohira and Y. Ito, *J. Am. Chem. Soc.*, 2003, **125**, 334–335.
- T. Murakami, T. Nohira, Y. Araki, T. Goto, R. Hagiwara and Y. H. Ogata, *Electrochem. Solid-State Lett.*, 2007, **10**, E4–E6.
- I. A. Amar, R. Lan and S. Tao, *RSC Adv.*, 2015, **5**, 38977–38983.
- S. Licht, B. Cui, B. Wang, F.-F. Li, J. Lau and S. Liu, *Science*, 2014, **345**, 637–640.
- F.-F. Li and S. Licht, *Inorg. Chem.*, 2014, **53**, 10042–10044.

- 40 S. Chen, S. Perathoner, C. Ampelli, C. Mebrahtu, D. Su and G. Centi, *Angew. Chem., Int. Ed.*, 2017, **56**, 2699–2703.
- 41 A. B. Djuricic, Y. H. Leung and A. M. Ching Ng, *Mater. Horiz.*, 2014, **1**, 400–410.
- 42 M. Marszewski, S. Cao, J. Yu and M. Jaroniec, *Mater. Horiz.*, 2015, **2**, 261–278.
- 43 Y. Ma, X. Wang, Y. Jia, X. Chen, H. Han and C. Li, *Chem. Rev.*, 2014, **114**, 9987–10043.
- 44 J. L. White, M. F. Baruch, J. E. Pander III, Y. Hu, I. C. Fortmeyer, J. E. Park, T. Zhang, K. Liao, J. Gu, Y. Yan, T. W. Shaw, E. Abelev and A. B. Bocarsly, *Chem. Rev.*, 2015, **115**, 12888–12935.
- 45 K. Wenderich and G. Mul, *Chem. Rev.*, 2016, **116**, 14587–14619.
- 46 Y. Zhao, X. Jia, G. I. N. Waterhouse, L.-Z. Wu, C.-H. Tung, D. O'Hare and T. Zhang, *Adv. Energy Mater.*, 2016, **6**, 1501974.
- 47 X. Liu, J. Iocozzia, Y. Wang, X. Cui, Y. Chen, S. Zhao, Z. Li and Z. Lin, *Energy Environ. Sci.*, 2017, **10**, 402–434.
- 48 A. Kudo and Y. Miseki, *Chem. Soc. Rev.*, 2009, **38**, 253–278.
- 49 L. K. Putri, B.-J. Ng, W.-J. Ong, H. W. Lee, W. S. Chang and S.-P. Chai, *ACS Appl. Mater. Interfaces*, 2017, **9**, 4558–4569.
- 50 W.-J. Ong, L.-L. Tan, S.-P. Chai, S.-T. Yong and A. R. Mohamed, *Nanoscale*, 2014, **6**, 1946–2008.
- 51 J. Di, J. Xia, H. Li and Z. Liu, *Nano Energy*, 2017, **35**, 79–91.
- 52 J. Yang, D. Wang, H. Han and C. Li, *Acc. Chem. Res.*, 2013, **46**, 1900–1909.
- 53 X. Chen, S. Shen, L. Guo and S. S. Mao, *Chem. Rev.*, 2010, **110**, 6503–6570.
- 54 S. Chen, T. Takata and K. Domen, *Nat. Rev. Mater.*, 2017, **2**, 17050.
- 55 Q. Lu, Y. Yu, Q. Ma, B. Chen and H. Zhang, *Adv. Mater.*, 2016, **28**, 1917–1933.
- 56 G. A. M. Hutton, B. C. M. Martindale and E. Reisner, *Chem. Soc. Rev.*, 2017, DOI: 10.1039/c7cs00235a.
- 57 G. Zhang, Z.-A. Lan and X. Wang, *Chem. Sci.*, 2017, **8**, 5261–5274.
- 58 X. Chang, T. Wang and J. Gong, *Energy Environ. Sci.*, 2016, **9**, 2177–2196.
- 59 S. J. A. Moniz, S. A. Shevlin, D. J. Martin, Z.-X. Guo and J. Tang, *Energy Environ. Sci.*, 2015, **8**, 731–759.
- 60 X. Meng, L. Liu, S. Ouyang, H. Xu, D. Wang, N. Zhao and J. Ye, *Adv. Mater.*, 2016, **28**, 6781–6803.
- 61 J. Li, H. Li, G. Zhan and L. Zhang, *Acc. Chem. Res.*, 2017, **50**, 112–121.
- 62 G. Dong, W. Ho and C. Wang, *J. Mater. Chem. A*, 2015, **3**, 23435–23441.
- 63 N. Dhar and S. Chowdhry, *Proc. Natl. Acad. Sci., India*, 1968, **38**, 485–490.
- 64 G. N. Schrauzer, N. Strampach, L. N. Hui, M. R. Palmer and J. Salehi, *Proc. Natl. Acad. Sci. U. S. A.*, 1983, **80**, 3873–3876.
- 65 A. J. Medford and M. C. Hatzell, *ACS Catal.*, 2017, **7**, 2624–2643.
- 66 G. N. Schrauzer, *Energy Efficiency and Renewable Energy Through Nanotechnology*, Springer, 2011, pp. 601–623.
- 67 G. N. Schrauzer and T. D. Guth, *J. Am. Chem. Soc.*, 1977, **99**, 7189–7193.
- 68 T. Bazhenova and A. Shilov, *Coord. Chem. Rev.*, 1995, **144**, 69–145.
- 69 C. J. van der Ham, M. T. Koper and D. G. Hetterscheid, *Chem. Soc. Rev.*, 2014, **43**, 5183–5191.
- 70 L.-j. Guo, Y.-j. Wang and T. He, *Chem. Rev.*, 2016, **16**, 1918–1933.
- 71 S. Sun, X. Li, W. Wang, L. Zhang and X. Sun, *Appl. Catal., B*, 2017, **200**, 323–329.
- 72 W. J. Ong, L. L. Tan, S. P. Chai, S. T. Yong and A. R. Mohamed, *ChemSusChem*, 2014, **7**, 690–719.
- 73 W.-J. Ong, L.-L. Tan, Y. H. Ng, S.-T. Yong and S.-P. Chai, *Chem. Rev.*, 2016, **116**, 7159–7329.
- 74 L. K. Putri, L.-L. Tan, W.-J. Ong, W. S. Chang and S.-P. Chai, *Appl. Mater. Today*, 2016, **4**, 9–16.
- 75 A. Fuertes, *Mater. Horiz.*, 2015, **2**, 453–461.
- 76 F. K. Kessler, Y. Zheng, D. Schwarz, C. Merschjann, W. Schnick, X. Wang and M. J. Bojdys, *Nat. Rev. Mater.*, 2017, **2**, 17030.
- 77 K. Sivula and R. van de Krol, *Nat. Rev. Mater.*, 2016, **1**, 16010.
- 78 I. Roger, M. A. Shipman and M. D. Symes, *Nat. Rev. Chem.*, 2017, **1**, 0003.
- 79 Y. Tachibana, L. Vayssieres and J. R. Durrant, *Nat. Photonics*, 2012, **6**, 511–518.
- 80 J. Low, J. Yu, M. Jaroniec, S. Wageh and A. A. Al-Ghamdi, *Adv. Mater.*, 2017, **29**, 1601694.
- 81 S. Cao, J. Low, J. Yu and M. Jaroniec, *Adv. Mater.*, 2015, **27**, 2150–2176.
- 82 H. Li, Y. Zhou, W. Tu, J. Ye and Z. Zou, *Adv. Funct. Mater.*, 2015, **25**, 998–1013.
- 83 L. K. Putri, W.-J. Ong, W. S. Chang and S.-P. Chai, *Appl. Surf. Sci.*, 2015, **358**(part A), 2–14.
- 84 S. Hoang and P.-X. Gao, *Adv. Energy Mater.*, 2016, **6**, 1600683.
- 85 X. Li, J. Yu and M. Jaroniec, *Chem. Soc. Rev.*, 2016, **45**, 2603–2636.
- 86 H. Li, J. Li, Z. Ai, F. Jia and L. Zhang, *Angew. Chem.*, 2017, DOI: 10.1002/ange.201705628.
- 87 L. M. Azofra, N. Li, D. R. MacFarlane and C. Sun, *Energy Environ. Sci.*, 2016, **9**, 2545–2549.
- 88 H. Li, J. Shang, J. Shi, K. Zhao and L. Zhang, *Nanoscale*, 2016, **8**, 1986–1993.
- 89 Y. Bai, L. Ye, T. Chen, L. Wang, X. Shi, X. Zhang and D. Chen, *ACS Appl. Mater. Interfaces*, 2016, **8**, 27661–27668.
- 90 A. Fujishima and K. Honda, *Nature*, 1972, **238**, 37–38.
- 91 S. Bourgeois, D. Diakite and M. Perdureau, *React. Solids*, 1988, **6**, 95–104.
- 92 H. Hirakawa, M. Hashimoto, Y. Shiraishi and T. Hirai, *J. Am. Chem. Soc.*, 2017, **139**, 10929–10936.
- 93 V. Augugliaro, A. Lauricella, L. Rizzuti, M. Schiavello and A. Sclafani, *Int. J. Hydrogen Energy*, 1982, **7**, 845–849.
- 94 Y. Iida and S. Ozaki, *J. Am. Ceram. Soc.*, 1961, **44**, 120–127.
- 95 J. Navio, M. Macias, M. Gonzalez-Catalan and A. Justo, *J. Mater. Sci.*, 1992, **27**, 3036–3042.
- 96 P. P. Radford and C. G. Francis, *J. Chem. Soc., Chem. Commun.*, 1983, 1520–1521.
- 97 M. Rao, K. Rajeshwar, V. P. Verneker and J. DuBow, *J. Phys. Chem.*, 1980, **84**, 1987–1991.
- 98 J. Soria, J. Conesa, V. Augugliaro, L. Palmisano, M. Schiavello and A. Sclafani, *J. Phys. Chem.*, 1991, **95**, 274–282.
- 99 W. Zhao, J. Zhang, X. Zhu, M. Zhang, J. Tang, M. Tan and Y. Wang, *Appl. Catal., B*, 2014, **144**, 468–477.

- 100 L. Palmisano, V. Augugliaro, A. Sclafani and M. Schiavello, *J. Phys. Chem.*, 1988, **92**, 6710–6713.
- 101 C. Martin, I. Martin, V. Rives, L. Palmisano and M. Schiavello, *J. Catal.*, 1992, **134**, 434–444.
- 102 O. Ieperuma, K. Tennakone and W. Dissanayake, *Appl. Catal.*, 1990, **62**, L1–L5.
- 103 O. Ieperuma, C. Thaminimulla and W. Kiridena, *Sol. Energy Mater. Sol. Cells*, 1993, **28**, 335–343.
- 104 H. Miyama, N. Fujii and Y. Nagae, *Chem. Phys. Lett.*, 1980, **74**, 523–524.
- 105 M. M. Taqui Khan, D. Chatterjee and M. Bala, *J. Photochem. Photobiol., A*, 1992, **67**, 349–352.
- 106 K. T. Ranjit, T. K. Varadarajan and B. Viswanathan, *J. Photochem. Photobiol., A*, 1996, **96**, 181–185.
- 107 O. P. Linnik and H. Kisch, *Mendeleev Commun.*, 2008, **18**, 10–11.
- 108 K. Hoshino, M. Inui, T. Kitamura and H. Kokado, *Angew. Chem., Int. Ed.*, 2000, **39**, 2509–2512.
- 109 K. Hoshino, *Chem. – Eur. J.*, 2001, **7**, 2727–2731.
- 110 K. Hoshino, R. Kuchii and T. Ogawa, *Appl. Catal., B*, 2008, **79**, 81–88.
- 111 M. M. Khader, N. N. Lichtin, G. H. Vurens, M. Salmeron and G. A. Somorjai, *Langmuir*, 1987, **3**, 303–304.
- 112 C. J. Jacobsen, S. Dahl, B. S. Clausen, S. Bahn, A. Logadottir and J. K. Nørskov, *J. Am. Chem. Soc.*, 2001, **123**, 8404–8405.
- 113 M. Lashgari and P. Zeinalkhani, *Appl. Catal., A*, 2017, **529**, 91–97.
- 114 E. Endoh, J. K. Leland and A. J. Bard, *J. Phys. Chem.*, 1986, **90**, 6223–6226.
- 115 W. Zhao, H. Xi, M. Zhang, Y. Li, J. Chen, J. Zhang and X. Zhu, *Chem. Commun.*, 2015, **51**, 4785–4788.
- 116 S. Sun, Q. An, W. Wang, L. Zhang, J. Liu and W. A. Goddard III, *J. Mater. Chem. A*, 2017, **5**, 201–209.
- 117 V. Augugliaro, F. D'alba, L. Rizzuti, M. Schiavello and A. Sclafani, *Int. J. Hydrogen Energy*, 1982, **7**, 851–855.
- 118 C. M. Janet, S. Navaladian, B. Viswanathan, T. K. Varadarajan and R. P. Viswanath, *J. Phys. Chem. C*, 2010, **114**, 2622–2632.
- 119 H. Pan, X. Meng and G. Qin, *Phys. Chem. Chem. Phys.*, 2014, **16**, 25442–25448.
- 120 D. Cordischi, N. Burriesci, F. D'Alba, M. Petrera, G. Polizzotti and M. Schiavello, *J. Solid State Chem.*, 1985, **56**, 182–190.
- 121 O. Rusina, A. Eremenko, G. Frank, H. P. Strunk and H. Kisch, *Angew. Chem., Int. Ed.*, 2001, **40**, 3993–3995.
- 122 O. Rusina, O. Linnik, A. Eremenko and H. Kisch, *Chem. – Eur. J.*, 2003, **9**, 561–565.
- 123 O. Linnik and H. Kisch, *Photochem. Photobiol. Sci.*, 2006, **5**, 938–942.
- 124 G. N. Schrauzer, T. D. Guth, J. Salehi, N. Strampach, N. H. Liu and M. R. Palmer, in *Homogeneous and Heterogeneous Photocatalysis*, ed. E. Pelizzetti and N. Serpone, Reidel, Hingham, MA, 1986, vol. 174, pp. 509–518.
- 125 Q.-s. Li, K. Domen, S. Naito, T. Onishi and K. Tamaru, *Chem. Lett.*, 1983, 321–324.
- 126 S. Linic, P. Christopher and D. B. Ingram, *Nat. Mater.*, 2011, **10**, 911–921.
- 127 T. Oshikiri, K. Ueno and H. Misawa, *Angew. Chem., Int. Ed.*, 2014, **53**, 9802–9805.
- 128 T. Oshikiri, K. Ueno and H. Misawa, *Angew. Chem.*, 2016, **128**, 4010–4014.
- 129 E. Skulason, T. Bligaard, S. Gudmundsdóttir, F. Studt, J. Rossmeisl, F. Abild-Pedersen, T. Vegge, H. Jónsson and J. K. Nørskov, *Phys. Chem. Chem. Phys.*, 2012, **14**, 1235–1245.
- 130 M. A. Shipman and M. D. Symes, *Catal. Today*, 2017, **286**, 57–68.
- 131 Y. Hao, X. Dong, S. Zhai, H. Ma, X. Wang and X. Zhang, *Chem. – Eur. J.*, 2016, **22**, 18722–18728.
- 132 K. Tennakone, S. Wickramanayake, C. Fernando, O. Ieperuma and S. Punchihewa, *J. Chem. Soc., Chem. Commun.*, 1987, 1078–1080.
- 133 K. Tennakone, J. Bandara, C. Thaminimulla, W. Jayatilake, U. Ketipearachchi, O. Ieperuma and M. Priyadarshana, *Langmuir*, 1991, **7**, 2166–2168.
- 134 K. Tennakone, S. Punchihewa and R. Tantrigoda, *Sol. Energy Mater.*, 1989, **18**, 217–221.
- 135 K. Tennakone, C. Thaminimulla and W. Kiridena, *Langmuir*, 1993, **9**, 723–726.
- 136 X. Li, W. Wang, D. Jiang, S. Sun, L. Zhang and X. Sun, *Chem. – Eur. J.*, 2016, **22**, 13819–13822.
- 137 O. Ieperuma, W. Kiridena and W. Dissanayake, *J. Photochem. Photobiol., A*, 1991, **59**, 191–197.
- 138 K. Tennakone, C. Fernando, S. Wickramanayake, M. Damayanthi, L. Silva, W. Wijeratne, O. Ieperuma and S. Punchihewa, *Sol. Energy Mater.*, 1988, **17**, 47–53.
- 139 K. Tennakone, C. Thaminimulla and J. Bandara, *J. Photochem. Photobiol., A*, 1992, **68**, 131–135.
- 140 W.-J. Ong, L. K. Putri, Y.-C. Tan, L.-L. Tan, N. Li, Y. H. Ng, X. Wen and S.-P. Chai, *Nano Res.*, 2017, **10**, 1673–1696.
- 141 X. Zong, H. Yan, G. Wu, G. Ma, F. Wen, L. Wang and C. Li, *J. Am. Chem. Soc.*, 2008, **130**, 7176–7177.
- 142 H. Yan, J. Yang, G. Ma, G. Wu, X. Zong, Z. Lei, J. Shi and C. Li, *J. Catal.*, 2009, **266**, 165–168.
- 143 S. Navalón, A. Dhakshinamoorthy, M. Álvaro and H. Garcia, *ChemSusChem*, 2013, **6**, 562–577.
- 144 M. M. T. Khan, R. C. Bhardwaj and C. Bhardwaj, *Angew. Chem., Int. Ed.*, 1988, **27**, 923–925.
- 145 M. T. Khan and N. N. Rao, *J. Mol. Catal. A: Chem.*, 1990, **58**, 323–329.
- 146 L. Ye, C. Han, Z. Ma, Y. Leng, J. Li, X. Ji, D. Bi, H. Xie and Z. Huang, *Chem. Eng. J.*, 2017, **307**, 311–318.
- 147 K. A. Brown, D. F. Harris, M. B. Wilker, A. Rasmussen, N. Khadka, H. Hamby, S. Keable, G. Dukovic, J. W. Peters and L. C. Seefeldt, *Science*, 2016, **352**, 448–450.
- 148 A. Banerjee, B. D. Yuhas, E. A. Margulies, Y. Zhang, Y. Shim, M. R. Wasielewski and M. G. Kanatzidis, *J. Am. Chem. Soc.*, 2015, **137**, 2030–2034.
- 149 J. Liu, M. S. Kelley, W. Wu, A. Banerjee, A. P. Douvalis, J. Wu, Y. Zhang, G. C. Schatz and M. G. Kanatzidis, *Proc. Natl. Acad. Sci. U. S. A.*, 2016, **113**, 5530–5535.
- 150 B. M. Hoffman, D. R. Dean and L. C. Seefeldt, *Acc. Chem. Res.*, 2009, **42**, 609–619.
- 151 H. Li, J. Shang, Z. Ai and L. Zhang, *J. Am. Chem. Soc.*, 2015, **137**, 6393–6399.
- 152 S. Hu, X. Chen, Q. Li, Y. Zhao and W. Mao, *Catal. Sci. Technol.*, 2016, **6**, 5884–5890.

- 153 Y. Cao, S. Hu, F. Li, Z. Fan, J. Bai, G. Lu and Q. Wang, *RSC Adv.*, 2016, **6**, 49862–49867.
- 154 S. Hu, Y. Li, F. Li, Z. Fan, H. Ma, W. Li and X. Kang, *ACS Sustainable Chem. Eng.*, 2016, **4**, 2269–2278.
- 155 Q. Zhang, S. Hu, Z. Fan, D. Liu, Y. Zhao, H. Ma and F. Li, *Dalton Trans.*, 2016, **45**, 3497–3505.
- 156 S. Wu, J. S. Ross, G.-B. Liu, G. Aivazian, A. Jones, Z. Fei, W. Zhu, D. Xiao, W. Yao, D. Cobden and X. Xu, *Nat. Phys.*, 2013, **9**, 149–153.
- 157 K. F. Mak, K. He, J. Shan and T. F. Heinz, *Nat. Nanotechnol.*, 2012, **7**, 494–498.
- 158 E. A. A. Pogna, M. Marsili, D. De Fazio, S. Dal Conte, C. Manzoni, D. Sangalli, D. Yoon, A. Lombardo, A. C. Ferrari, A. Marini, G. Cerullo and D. Prezzi, *ACS Nano*, 2016, **10**, 1182–1188.
- 159 S. Sun, X. Li, W. Wang, L. Zhang and X. Sun, *Appl. Catal., B*, 2017, **200**, 323–329.
- 160 C. H. Lui, A. J. Frenzel, D. V. Pilon, Y. H. Lee, X. Ling, G. M. Akselrod, J. Kong and N. Gedik, *Phys. Rev. Lett.*, 2014, **113**, 166801.
- 161 H. Cheng, B. Huang and Y. Dai, *Nanoscale*, 2014, **6**, 2009–2026.
- 162 W. L. Huang and Q. Zhu, *J. Comput. Chem.*, 2009, **30**, 183–190.
- 163 X. Y. Kong, W. Lee, W. J. Ong, S. P. Chai and A. R. Mohamed, *ChemCatChem*, 2016, **8**, 3074–3081.
- 164 S. Wang, X. Hai, X. Ding, K. Chang, Y. Xiang, X. Meng, Z. Yang, H. Chen and J. Ye, *Adv. Mater.*, 2017, **29**, 1701774.
- 165 D. Zhu, L. Zhang, R. E. Ruther and R. J. Hamers, *Nat. Mater.*, 2013, **12**, 836–841.
- 166 J. R. Christianson, D. Zhu, R. J. Hamers and J. R. Schmidt, *J. Phys. Chem. B*, 2014, **118**, 195–203.
- 167 J. A. Bandy, D. Zhu and R. J. Hamers, *Diamond Relat. Mater.*, 2016, **64**, 34–41.
- 168 H. Ma, Z. Shi, S. Li and N. Liu, *Appl. Surf. Sci.*, 2016, **379**, 309–315.
- 169 S. Li, X. Chen, S. Hu, Q. Li, J. Bai and F. Wang, *RSC Adv.*, 2016, **6**, 45931–45937.
- 170 H. Ma, Z. Shi, Q. Li and S. Li, *J. Phys. Chem. Solids*, 2016, **99**, 51–58.
- 171 G. Wu, Y. Gao and B. Zheng, *Ceram. Int.*, 2016, **42**, 6985–6992.
- 172 S. Hu, X. Chen, Q. Li, F. Li, Z. Fan, H. Wang, Y. Wang, B. Zheng and G. Wu, *Appl. Catal., B*, 2017, **201**, 58–69.
- 173 Z. Ma, S. Zhao, X. Xiong, B. Hu and C. Song, *Catal. Lett.*, 2016, **146**, 2324–2329.
- 174 Y. Wang, W. Wei, M. Li, S. Hu, J. Zhang and R. Feng, *RSC Adv.*, 2017, **7**, 18099–18107.
- 175 H. Liang, H. Zou and S. Hu, *New J. Chem.*, 2017, **41**, 8920–8926.
- 176 S. Cao, N. Zhou, F. Gao, H. Chen and F. Jiang, *Appl. Catal., B*, 2017, **218**, 600–610.
- 177 S. Hu, W. Zhang, J. Bai, G. Lu, L. Zhang and G. Wu, *RSC Adv.*, 2016, **6**, 25695–25702.
- 178 S. Hu, F. Li, Z. Fan, F. Wang, Y. Zhao and Z. Lv, *Dalton Trans.*, 2015, **44**, 1084–1092.
- 179 Q. Han, N. Chen, J. Zhang and L. Qu, *Mater. Horiz.*, 2017, **4**, 832–850.
- 180 W.-J. Ong, L.-L. Tan, S.-P. Chai and S.-T. Yong, *Chem. Commun.*, 2015, **51**, 858–861.
- 181 W.-J. Ong, L.-L. Tan, S.-P. Chai, S.-T. Yong and A. R. Mohamed, *Nano Energy*, 2015, **13**, 757–770.
- 182 W.-J. Ong, *Front. Mater.*, 2017, **4**, 11, DOI: 10.3389/fmats.2017.00011.
- 183 Y. Lu, Y. Yang, T. Zhang, Z. Ge, H. Chang, P. Xiao, Y. Xie, L. Hua, Q. Li and H. Li, *ACS Nano*, 2016, **10**, 10507–10515.
- 184 Y. Yang, T. Zhang, Z. Ge, Y. Lu, H. Chang, P. Xiao, R. Zhao, Y. Ma and Y. Chen, *Carbon*, 2017, **124**, 72–78.
- 185 P. Dean, *Phys. Rev.*, 1967, **157**, 655.
- 186 B. Aurian-Blajeni, M. Halmann and J. Manassen, *Sol. Energy Mater.*, 1983, **8**, 425–440.
- 187 C. R. Dickson and A. J. Nozik, *J. Am. Chem. Soc.*, 1978, **100**, 8007–8009.
- 188 F. Khan, P.-L. Yue, L. Rizzuti, V. Augugliaro and M. Schiavello, *J. Chem. Soc., Chem. Commun.*, 1981, **20**, 1049–1050.
- 189 F. Khan, P. Yue, L. Rizzuti, V. Augugliaro and A. Brucato, *Ind. Eng. Chem. Res.*, 1983, **22**, 238–241.
- 190 H. Zeng, S. Terazono and T. Tanuma, *Catal. Commun.*, 2015, **59**, 40–44.
- 191 M. Ali, F. Zhou, K. Chen, C. Kotzur, C. Xiao, L. Bourgeois, X. Zhang and D. R. MacFarlane, *Nat. Commun.*, 2016, **7**, 11335.
- 192 L. Li, Y. Wang, S. Vanka, X. Mu, Z. Mi and C.-J. Li, *Angew. Chem.*, 2017, **129**, 8827–8831.
- 193 A. Klerke, C. H. Christensen, J. K. Nørskov and T. Vegge, *J. Mater. Chem.*, 2008, **18**, 2304–2310.
- 194 R. Lan, J. T. S. Irvine and S. Tao, *Int. J. Hydrogen Energy*, 2012, **37**, 1482–1494.
- 195 W.-J. Ong, L. K. Putri, L.-L. Tan, S.-P. Chai and S.-T. Yong, *Appl. Catal., B*, 2016, **180**, 530–543.
- 196 D. Zeng, W.-J. Ong, H. Zheng, M. Wu, Y. Chen, D.-L. Peng and M. Han, *J. Mater. Chem. A*, 2017, **5**, 16171–16178.
- 197 L. K. Putri, W.-J. Ong, W. S. Chang and S.-P. Chai, *Catal. Sci. Technol.*, 2016, **6**, 744–754.
- 198 D. Zeng, L. Xiao, W.-J. Ong, P. Wu, H. Zheng, Y. Chen and D.-L. Peng, *ChemSusChem*, 2017, DOI: 10.1002/cssc.201701345.
- 199 W.-J. Ong, L.-L. Tan, S.-P. Chai and S.-T. Yong, *Dalton Trans.*, 2015, **44**, 1249–1257.
- 200 D. Zeng, W. Xu, W.-J. Ong, J. Xu, H. Ren, Y. Chen, H. Zheng and D.-L. Peng, *Appl. Catal., B*, 2017, DOI: 10.1016/j.apcatb.2017.08.041.
- 201 W.-J. Ong, L.-L. Tan, S.-P. Chai, S.-T. Yong and A. R. Mohamed, *Nano Res.*, 2014, **7**, 1528–1547.
- 202 L. J. Guo, Y. J. Wang and T. He, *Chem. Rec.*, 2016, **16**, 1918–1933.
- 203 P. Qiu, C. Xu, N. Zhou, H. Chen and F. Jiang, *Appl. Catal., B*, 2017, DOI: 10.1016/j.apcatb.2017.09.010.